The SON RNA splicing factor is required for intracellular trafficking structures that promote centriole assembly and ciliogenesis

Alexander J. Stemm-Wolf[a], Eileen T. O'Toole[b], Ryan M. Sheridan[c], Jacob T. Morgan[a], and Chad G. Pearson[a,*]

[a]Department of Cell and Developmental Biology, University of Colorado, Anschutz Medical Campus, Aurora, CO 80045; [b]MCDB, University of Colorado, Boulder, Boulder, CO; [c]RNA Biosciences Initiative (RBI), University of Colorado, Anschutz Medical Campus, Aurora, CO 80045

ABSTRACT Control of centrosome assembly is critical for cell division, intracellular trafficking, and cilia. Regulation of centrosome number occurs through the precise duplication of centrioles that reside in centrosomes. Here we explored transcriptional control of centriole assembly and find that the RNA splicing factor SON is specifically required for completing procentriole assembly. Whole genome mRNA sequencing identified genes whose splicing and expression are affected by the reduction of SON, with an enrichment in genes involved in the microtubule (MT) cytoskeleton, centrosome, and centriolar satellites. SON is required for the proper splicing and expression of *CEP131*, which encodes a major centriolar satellite protein and is required to organize the trafficking and MT network around the centrosomes. This study highlights the importance of the distinct MT trafficking network that is intimately associated with nascent centrioles and is responsible for procentriole development and efficient ciliogenesis.

INTRODUCTION

Centrosomes are major nucleators and organizers of microtubules (MTs) in dividing cells. Within the centrosome, a pair of MT-based centrioles serve both to recruit the surrounding pericentriolar material (PCM) necessary for MT nucleation and to facilitate control of centrosome assembly such that cells have one centrosome at the beginning of the cell cycle and two centrosomes prior to cell division. This promotes the assembly of a bipolar spindle during mitosis, thus ensuring high-fidelity segregation of chromosomes to daughter cells (Loncarek and Bettencourt-Dias, 2018; Nigg and Holland, 2018). Fully mature centrioles also act as nucleators and anchors for primary cilia which are required for signaling pathways critical during development (Mitchison and Valente, 2017). Dysregulation of centrosome number can instigate cellular transformation to a cancerous state (Levine et al., 2017). More than two centrosomes results in chromosomal instability (Ganem et al., 2009; Silkworth et al., 2009; Zhang et al., 2015), altered cell migration (Godinho et al., 2014) and disruptions to the MT network (Godinho et al., 2014; Marteil et al., 2018; Sankaran et al., 2020). Differentiated cells, on the other hand, often utilize noncentrosomal MT organizing centers (MTOCs) and must attenuate the MT nucleating function of the centrosome (Sanchez and Feldman, 2017), suggesting the existence of broad programs to regulate MTOC activity. Control of centriole assembly and centrosome activity, therefore, has profound implications for development and disease.

Centriole assembly occurs in distinct stages: assembly is stimulated by the activity of the PLK4 kinase which coordinates the addition of early structural factors that establish the ninefold symmetry of the structure at its proximal end (Kleylein-Sohn et al., 2007; Kitagawa et al., 2011). Additional factors, such as centrobin, CPAP, and POC5, are required for centriole elongation (Azimzadeh et al., 2009; Schmidt et al., 2009; Gudi et al., 2011; Lin et al., 2013b). Protein components required for assembling centrioles traffic in cytoplasmic particles associated both with the centrosome scaffold protein,

pericentrin (PCNT), and with centriolar satellites (Dammermann and Merdes, 2002; Hori *et al.*, 2015; Kodani *et al.*, 2015; Ito *et al.*, 2019; Prosser and Pelletier, 2020). Both PCNT granules and centriolar satellites require MTs and dynein for their accumulation near the centrosome (Kubo *et al.*, 1999; Young *et al.*, 2000). Each stage of the centriole assembly process is a potential target for regulation of nascent centriole assembly.

Centrosome number is controlled by a multifaceted regulation of centriole duplication coordinated with the cell cycle. This includes PLK1-dependent licensing during mitotic exit that promotes centriole disengagement (Tsou *et al.*, 2009; Schöckel *et al.*, 2011; Matsuo *et al.*, 2012; Colicino and Hehnly, 2018). In S phase, the centriole assembly master regulator, PLK4, initiates early steps in procentriole assembly promoting the removal of the centriole assembly inhibitor Cdc6 (Xu *et al.*, 2017) and focusing centriole assembly to a single site on the mother centriole (Leda *et al.*, 2018; Park *et al.*, 2019; Yamamoto and Kitagawa, 2019). Interactions between PLK4 and STIL serve to stimulate PLK4 kinase activity and STIL phosphorylation by PLK4, allowing STIL to interact with the other early centriole assembly factors, SAS-6 and CPAP, initiating the assembly of the early procentriole (Moyer *et al.*, 2015; Liu *et al.*, 2018; McLamarrah *et al.*, 2018; Ohta *et al.*, 2018; Moyer and Holland, 2019). Furthermore, PLK4 phosphorylates the major centriolar satellite components CEP131 and PCM1, and PLK4-dependent phosphorylation of PCM1 is required for pericentrosomal localization of centriolar satellites (Hori *et al.*, 2016; Kim *et al.*, 2019), suggesting that trafficking of assembly factors to the centrosome may also be controlled by PLK4 regulation.

Although posttranslational modifications of proteins are critical in coordinating the regulated assembly of centrioles, they are not the only means of control employed by cells. Centriole assembly is also regulated at the posttranscriptional level where distinct mRNA isoforms both promote and repress nascent centriole assembly. Cell cycle controlled alternative polyadenylation of *CEP135* mRNA generates a short isoform of this centriole assembly factor, antagonizing the positive effects of the full-length isoform on centriole assembly (Dahl *et al.*, 2015; Ganapathi Sankaran *et al.*, 2019). This also correlates with centrosome amplification in cancer cells that have an overabundance of the long *CEP135* isoform relative to the short isoform (Ganapathi Sankaran *et al.*, 2019). Many additional genes important for cell cycle progression generally, and centriole assembly in particular, have been identified as alternatively spliced in a cell cycle-dependent manner (Dominguez *et al.*, 2016). The proper splicing of the γ-tubulin complex member, TUBGCP6, facilitated by WBP11, is required for centriole assembly (Park *et al.*, 2020). Additionally, multiple mRNA splicing factors were identified in a genomewide screen for genes required for centriole assembly and centriole number control (Balestra *et al.*, 2013). Together, these examples point to the importance of transcript-level regulation in the control of centriole assembly. Yet, how specific splicing regulators affect centriole assembly remains poorly understood.

The multidomained nuclear speckle and splicing factor protein, SON (Hickey *et al.*, 2014; Ilik *et al.*, 2020), is required for centriole assembly (Balestra *et al.*, 2013). SON is required for progression through the cell cycle and affects the efficient splicing of a number of genes important for MT nucleation and maintenance including γ-tubulin and PCNT (Huen *et al.*, 2010; Ahn *et al.*, 2011; Sharma *et al.*, 2011). Loss of function mutations in SON is associated with intellectual disability, facial dysmorphology, scoliosis, heart defects, and vision impairment, which are reminiscent of phenotypes associated with ciliopathies and could indicate defects in centriolar function and ciliogenesis (Kim *et al.*, 2016; Tokita *et al.*, 2016; Reiter and Leroux, 2017).

Here we demonstrate that SON is required for centriole assembly, independent of its effects on the cell cycle. Among its many splicing targets, as revealed by mRNA-sequencing, is the gene encoding the centriolar satellite protein CEP131 whose reduction leads to severe loss of centriolar satellites. We find that centriolar satellites have an intimate relationship to assembling centrioles, adding to the evidence that centriolar satellites contribute to centriole assembly (Hori *et al.*, 2015). Interestingly, *CEP131* has previously been identified as a target of the splicing factor NRDE2 (Jiao *et al.*, 2019), suggesting that regulation of *CEP131* transcript formation has an important role in centriolar satellite formation and function. Splicing of *PCNT* pre-mRNA utilizes SON (Ahn *et al.*, 2011). Interestingly, the trafficking population of PCNT surrounding centrosomes is severely disrupted by SON depletion. SON is required for the MT architecture around the interphase centrosomes; its absence radically changes the number and distribution of MTs around the centrosome and the makeup of the pericentrosomal region. This appears to be orchestrated by a transfer of MT nucleation activity from mother centrioles to their nascent daughters, facilitating the completion of procentriole assembly. As SON changes the distribution of MTs, centriolar satellites and other trafficking particles around centrosomes, and centriolar satellites promote efficient ciliogenesis (Odabasi *et al.*, 2019), we find that SON is also required for efficient cilium assembly. This study highlights the importance of alternative splicing in modulating centriole assembly and MT organization, suggesting a multifactorial mechanism by which cells can modulate centrosome duplication and ciliogenesis, which are critical for cell division and development.

RESULTS
The SON RNA splicing factor is required for centriole assembly

To explore the connection between centriole assembly and mRNA splicing, we selected five splicing factors from 14 that were identified in a global RNA interference screen for genes required for centriole assembly (Balestra *et al.*, 2013). Some have roles in cell cycle progression (SON and PRPF8; Ahn *et al.*, 2011; Wickramasinghe *et al.*, 2015), regulation of alternative splicing (SON and PNN; Chiu and Ouyang, 2006; Hickey *et al.*, 2014), and assembly of core splicing snRNP complexes (SNRPD2 and SF3A3; Urlaub *et al.*, 2001; Tanackovic and Krämer, 2005; Siebring-van Olst *et al.*, 2017). We first asked whether knockdown of these splicing factors limited centriole assembly in an hTERT immortalized retinal epithelial cell line (RPE-1), which more closely mimics noncancerous centriole assembly control, in a manner similar to the previously performed knockdown in a cancer-derived cell line (HeLa) (Balestra *et al.*, 2013). We employed an RPE-1 strain with GFP-tagged *CETN2* to identify centrioles by centrin fluorescence in cycling cells, and PLK4 under control of the rtTA, doxycycline inducible promoter (Gossen *et al.*, 1995; Hatch *et al.*, 2010), and counted centrioles following 48 h of splicing factor siRNA depletion (without PLK4 induction) (Figure 1A). Under these conditions, knockdown of SON, PNN and SNRPD2 demonstrated a significant decrease in the number of centrioles per cell, whereas knockdown of SF3A3 and PRPF8 had no observable effect on centriole frequency (Figure 1B).

Splicing factors are commonly required for generating mRNAs necessary for many cellular functions and often affect the cell cycle (Ahn *et al.*, 2011; Suvorova *et al.*, 2013; Kurokawa *et al.*, 2014; Abramczuk *et al.*, 2017). Centriole assembly is intimately linked to the cell cycle, and thus alterations to the cell cycle could affect centriole numbers in a manner indirectly related to centriole assembly control. To address this, we isolated centriole assembly from other
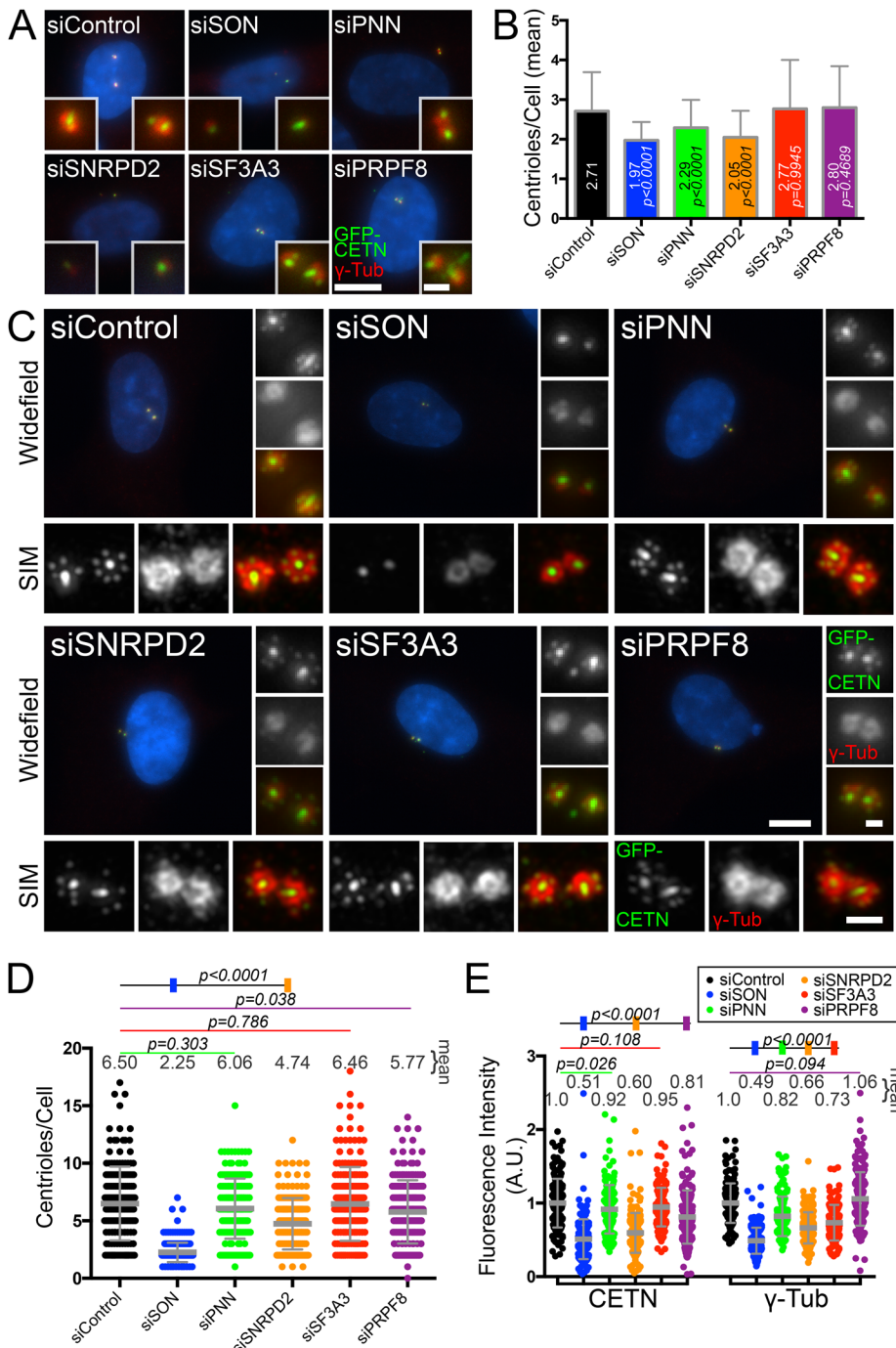
FIGURE 1: SON splicing factor depletion inhibits centriole assembly. (A) SON depletion reduces centriole duplication in cycling cells. Cycling RPE-1/GFP-Cetn/Tet-PLK4 cells without PLK4 induction treated with the indicated siRNAs for 48 h. Green, GFP-Cetn; red, γ-tubulin; blue, DNA. (B) Mean number of centrioles per cell. Mean and *p* values are indicated within the bars of the graph and *p* values are compared with siControl. *N* = siControl, 169 cells; siSON, 173 cells; siPNN, 173 cells; siSNRPD2, 169 cells; siSF3A3, 170 cells; siPRPF8, 180 cells. (C) SON depletion reduces centriole duplication in S phase-arrested and PLK4-induced cells. siRNA-treated, S phase-arrested cells induced for PLK4 expression. Top panels, widefield images; bottom panels, SIM images. (D) The number of centrioles per cell after S phase arrest and PLK4 induction. (E) Fluorescence quantification of GFP-Cetn and γ-tubulin within a 1-μm radius circle after S phase arrest and PLK4 induction. Scale bars for whole cells = 10 μm, for centrosomes = 1 μm. N for D and E = siControl, 177 cells; siSON, 204 cells; siPNN, 194 cells; siSNRPD2, 189 cells; siSF3A3, 195 cells; siPRPF8, 203 cells. Data were compiled from two biological replicates. Bar and error bars, mean and SD.

processes by observing cells under conditions of S phase arrest with overexpression of PLK4 to promote centriole assembly and more directly query centriole assembly defects (Figure 1C) (Kleylein-Sohn *et al.*, 2007). In 72% of cells, PLK4 induction results in procentriole assembly around the mother centriole, often in a rosette formation (Kleylein-Sohn *et al.*, 2007). GFP-centrin foci counts of cells under these conditions revealed that knockdown of SON and SNRPD2 resulted in significant reductions to centriole number when cell cycle effects were minimized. SON knockdown had by far the strongest effect, as only 2% of cells have procentrioles, based on GFP-centrin labeling (Figure 1D). Fluorescence quantification of GFP-centrin showed reduced levels with SON knockdown, commensurate with the reduction in centriole number (Figure 1E). GFP-centrin was also reduced with SNRPD2 knockdown and to a lesser extent with PRPF8 knockdown, suggesting that these proteins affect the amount of centrin protein present in daughter centrioles. Quantification of γ-tubulin fluorescence intensity did not completely correlate with GFP-centrin fluorescence, suggesting that different splicing factors affect centrosomal proteins in distinct ways (Figure 1E, see siSF3A3 and siPRPF8). Consistent with the reduction in γ-tubulin observed with SON knockdown, SON has previously been shown to be a splicing factor important for intron removal in *TUBG1* (γ-tubulin encoding gene) and affects γ-tubulin protein levels (Ahn *et al.*, 2011). We confirmed the SON siRNA knockdown (Supplemental Figure S1A) and the dramatic impact on daughter centriole assembly in SON knockdown with a second siRNA (Supplemental Figure S1B). Furthermore, aphidicolin-induced S phase arrest in *SON* knockdown cells reduced the number of cells with G2/M DNA content and brought the number of cells with DNA contents reflective of G1 and S phase to levels similar to that of siControl cells (Supplemental Figure S1C). Because PLK4 induction leads to centriole assembly initiation in under 1 h and its effects are not limited to S phase of the cell cycle (Kleylein-Sohn *et al.*, 2007), it is unlikely that differences in time spent in S phase are responsible for the centriole assembly defect observed on SON depletion. The SON centriole assembly defect is not due to a problem responding to doxycycline-induced PLK4 overexpression, as S phase-arrested cells without PLK4 induction have a centriole assembly defect (Supplemental Figure S1, D and E), as do cycling
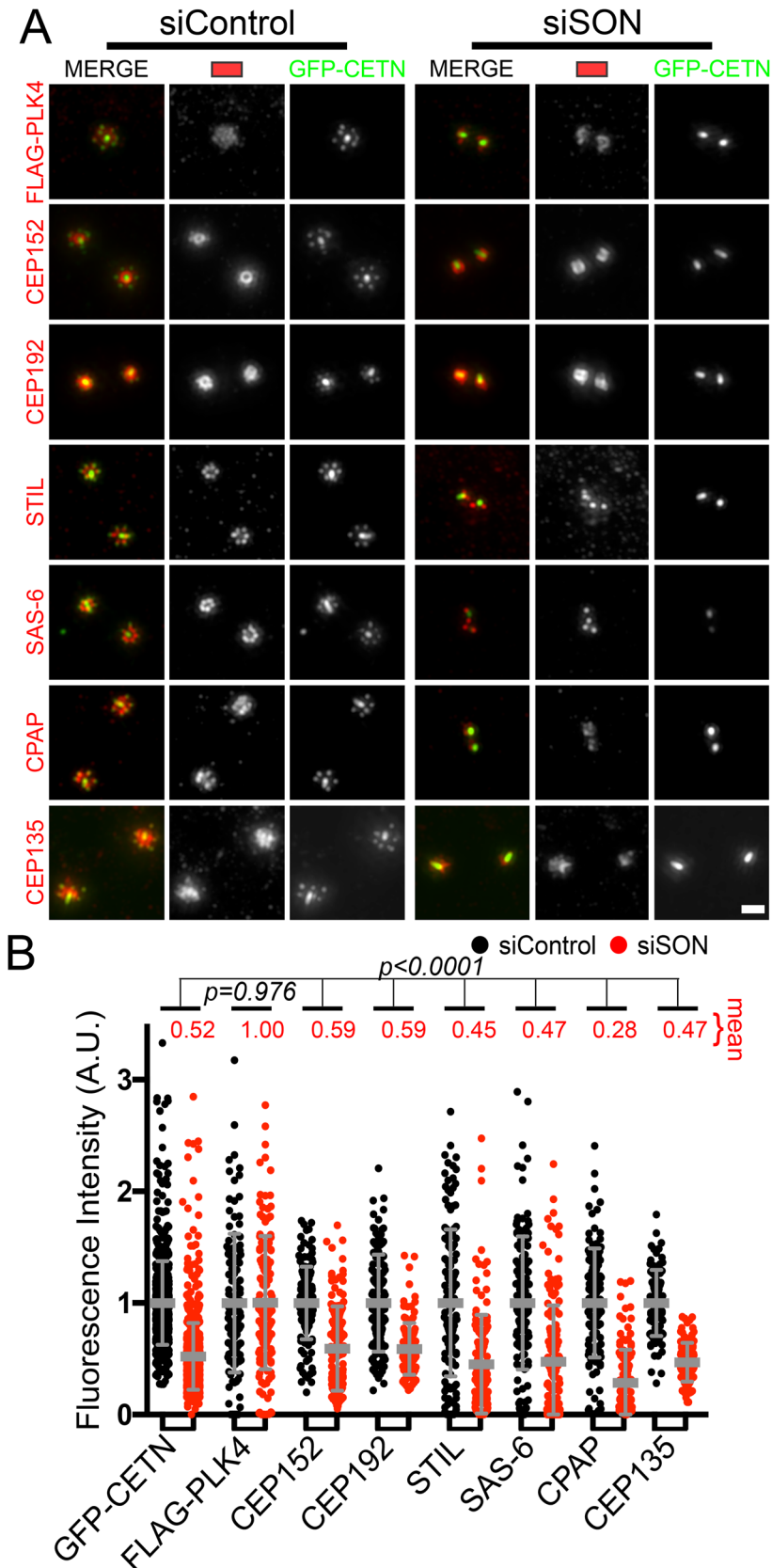
FIGURE 2: SON depletion reduces but does not eliminate early centriole assembly. (A) SIM images of siRNA-treated, S phase-arrested cells induced for PLK4 expression and stained for centriole assembly factors. Scale bar = 1 μm. (B) Fluorescence intensity quantifications within a 1-μm radius circle of widefield microscopy images (Supplemental Figure S2A). N = GFP-Cetn: siControl, 851 centrosomes; siSON, 925

cells observed in mitosis (Supplemental Figure S1, F and G). Because depletion of SON reduces centriole assembly independent of the cell cycle, we focused on this splicing factor asking which steps of centriole assembly are disrupted.

SON depletion is permissive for early steps of centriole assembly

Given that SON depletion abrogates procentriole assembly as determined by GFP-centrin incorporation, we examined the initiating events of centriole assembly upon SON depletion. Early centriole assembly events are known targets of posttranslational modification, particularly by PLK4 (Gönczy and Hatzopoulos, 2019), and the early centriole assembly component CEP135 is regulated posttranscriptionally (Dahl *et al.*, 2015). This led us to examine the localization of early centriole assembly proteins. CEP152 and CEP192 are centriole scaffold proteins that interact with and are required for PLK4 recruitment to the centriole (Kim *et al.*, 2013; Sonnen *et al.*, 2013). Total CEP152 and CEP192 are reduced at the centrosome in siSON (59% of siControl for both), but the mother centriole levels are only reduced to 75% of controls, suggesting that some of the reduction in protein levels is due to a lack of recruitment to procentrioles (Figure 2, A and B; Supplemental Figure S2B). Despite reductions of these scaffold proteins, levels of PLK4 at the centrosome are unaffected, suggesting that the defect in centriole assembly is not due to a failure to recruit PLK4 (Figure 2, A and B).

Assembly of new centrioles begins with STIL phosphorylation by PLK4, allowing for SAS-6 recruitment to nascent daughter centrioles where it forms the inner cartwheel, an early assembly intermediate in centriole assembly (Ohta *et al.*, 2014; Moyer and Holland, 2019). CPAP and CEP135 promote the connection of the cartwheel to the MT triplet walls of the growing centriole (Lin *et al.*, 2013a). We asked whether the levels of these early assembly factors are altered upon SON depletion, and if so, whether these alterations could result in the observed centriole assembly defect. The mean levels of these early assembly factors are reduced in siSON (Figure 2B, STIL = 45%, SAS-6 = 47%, CPAP = 28%, and CEP135 = 47%), but because mother centrioles were not resolved from daughter centrioles in these fluorescence quantification experiments, the difference in levels upon SON depletion could reflect a lack of protein at mother centrioles or a reduction in the number of daughter centrioles. However, in no

centrosomes; FLAG-PLK4: siControl, 111 centrosomes; siSON, 131 centrosomes; CEP152: siControl, 136 centrosomes; siSON, 143 centrosomes; CEP192: siControl, 124 centrosomes; siSON, 123 centrosomes; STIL: siControl, 136 centrosomes; siSON 138 centrosomes; SAS-6: siControl, 132 centrosomes; siSON, 148 centrosomes; CPAP: siControl, 120 centrosomes; siSON, 122 centrosomes; Cep135: siControl, 91 centrosomes; siSON, 119 centrosomes. Data were compiled from two biological replicates. Bar and error bars: mean and SD.

case did the abundance of any of these proteins correlate with more centriole assembly in individual cells in the siSON condition (Supplemental Figure S2, A and C). As expected in siControl-treated cells, both STIL and SAS-6 protein levels correlate with the number of centrioles as overexpression of either is sufficient to promote centriole assembly (Supplemental Figure S2C) (Leidel et al., 2005; Vulprecht et al., 2012). These data indicate that early centriole assembly factors are reduced but not eliminated during SON depletion. Furthermore, because a sufficient amount of these assembly factors in individual siSON cells does not correlate with more centrioles, these data suggest that their overall decrease in abundance is not responsible for the centriole assembly phenotype.

To ascertain whether centriole assembly initiates when SON is depleted, we examined SAS-6 levels. Because SAS-6 is lost from mature centrioles during exit from mitosis, SAS-6 signal exclusively marks assembling procentrioles (Puklowski et al., 2011). When PLK4 is induced, 13.6% of siControl-treated cells have two or fewer centrioles based on GFP-centrin foci indicating an absence of new centriole assembly (Supplemental Figure S3). We utilized this number to estimate a SAS-6 fluorescence intensity cut-off for new centriole assembly based on the 13.6 percentile of SAS-6 signal; 56% of siSON cells had a SAS-6 signal above this threshold. This suggests that more than half the SON-depleted cells have initiated centriole assembly (Supplemental Figure S3). We then utilized structured illumination microscopy (SIM) to examine siSON cells to determine whether early assembly factors were indeed present in a rosette configuration consistent with early procentriole assembly. Rosettes of STIL, SAS-6, CPAP, and CEP135 were detected around mother centrioles, even though no GFP–centrin-labeled procentriolar foci were observed (Figure 3A). This indicates that centriole assembly initiates in SON knockdown cells but is unable to proceed to completion.

To determine the structural events associated with these new procentriole assemblies, we used electron tomography. Consistent with the immunofluorescence data, when SON is depleted, three out of four cells examined exhibited incomplete procentriole rosettes with procentrioles that were on average shorter than those observed in control cells (Figure 3, B and C). Moreover, the MTs in these procentrioles lack the C-tubule which is present in control conditions (Figure 3B insets; Supplemental Movies S1 and S2). We therefore conclude that SON depletion prevents daughter centriole assembly at a stage after early procentriole assembly and initial MT nucleation events, but prior to complete triplet MT formation, centrin deposition, and centriole elongation.

SON impacts splicing of genes encoding centriolar satellite and MT proteins

To determine SON splicing targets responsible for the centriole assembly defect, we utilized global mRNA sequencing of RNA isolated from cells under conditions of S phase arrest and PLK4 induction. From these data, we identified 4413 genes down-regulated in SON-depleted cells (Supplemental Table S1). To establish whether SON has a greater effect on specific cellular structures, we identified Cellular Component (CC) Gene Ontology (GO) terms most effected by SON depletion. The most highly enriched GO terms include the MT cytoskeleton and centrosome (Figure 4A, Supplemental Table S1), which is consistent with the MT disruption previously observed after SON knockdown (Ahn et al., 2011; Sharma et al., 2011). Along with changes to expression levels, we also examined changes in alternative splicing using the software packages MAJIQ (Supplemental Table S2) (Vaquero-Garcia et al., 2016) and rMATS (Supplemental Table S3) (Shen et al., 2014). From this analysis we found 2996 genes by MAJIQ and 3531 genes by rMATS that showed significant
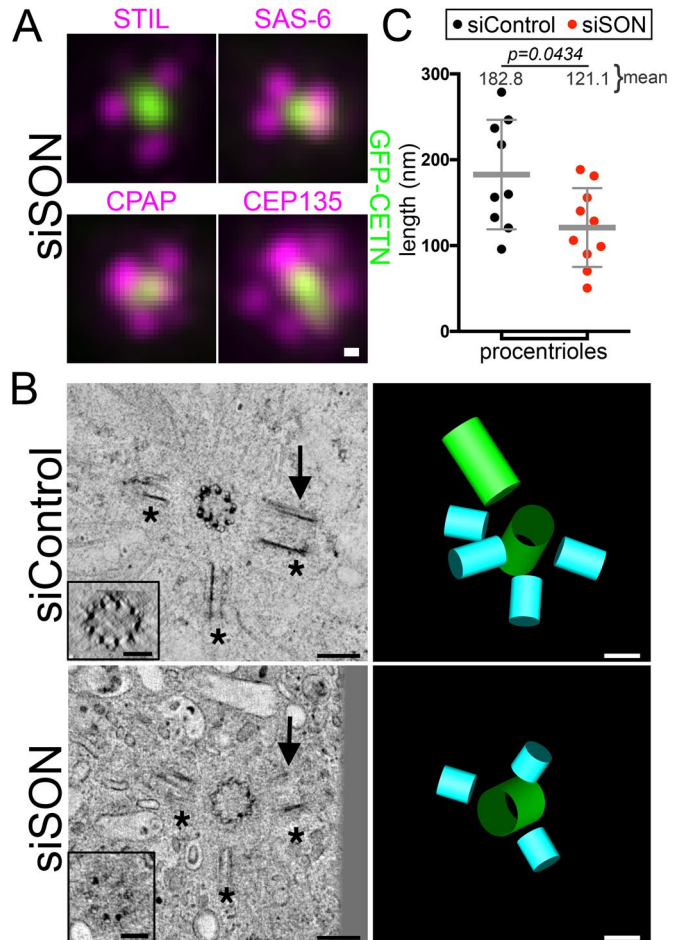

FIGURE 3: SON depletion causes short and immature procentrioles with missing C-tubules. (A) SIM images of siSON-treated cells stained as indicated showing that proteins required for early steps of procentriole assembly are present. Scale bar = 100 nm. (B) Tomographic slices and the corresponding tomographic models from siControl and siSON-treated cells. Procentrioles are present in both conditions and represented in blue in the models (asterisks indicate three of the fours procentrioles in siControl that are visible in this view). The arrows indicate the position of procentrioles that were rotated to reveal MT triplets in the control and MT doublets when SON is depleted (insets). The A-tubules are densely stained. The 3D model of the siControl rosette shows two mature centrioles (green) and Supplemental Movie S1 shows the complete volume built from four 250-nm-thick sections. The siSON centrosomes are separated and the adjacent centrosome is presented in Supplemental Figure S7A (D"). Supplemental Movie S2 shows the complete volume, which contains both centrosomes, and is built from four 250-nm-thick sections. Scale bars = 200 nm and 100 nm for insets. (C) The length of procentrioles in tomographic volumes. N = siControl, 9 procentrioles; siSON, 10 procentrioles. Bar and error bars: mean and SD.

changes in alternative splicing (Figure 4B). These two software packages identified genes with considerable overlap (74.3% of MAJIQ identified genes in the rMATS set and 63.1% rMATS identified genes in the MAJIQ set; Supplemental Figure S4A). These genes also showed strong enrichment for MT-associated GO terms including MT cytoskeleton, MTOC, centrosome, and centriole (Figure 4A). To investigate additional targets of SON that could contribute to the centriole assembly defect, we tested for overlap with genes encoding proteins included in the Centrosome Database (CD, portion of

the Centrosome and Cilia Database [CCDB; Gupta *et al.*, 2015]) and centriolar satellites (Gheiratmand *et al.*, 2019). Interestingly, differentially spliced genes strongly overlapped with both of these lists, indicating they are affected at a high rate by SON knockdown (Figure 4, A and B).

Genes from the CD and satellite proximity lists whose splicing is affected by SON were then sorted by their differential expression (Supplemental Table S4). Within the top 50 genes in this list were several with known functions at centrosomes, including *TUBG1* (γ-tubulin), *PCNT*, *CEP131*, *HAUS4* (augmin complex member), and *CNTROB* (centrobin) (Zou *et al.*, 2005; Delaval and Doxsey, 2010; Staples *et al.*, 2012; Thawani *et al.*, 2019). Intron excision events in *TUBG1* and *PCNT* had previously been reported as defective with SON depletion (Ahn *et al.*, 2011), and splicing changes to *CEP131* were detected in a microarray analysis (Sharma *et al.*, 2011). To verify changes to *CNTROB* and *CEP131* splicing on SON reduction, reverse transcription followed by PCR was performed. In addition to reducing the amount of *CNTROB* and *CEP131* mRNA, changes in alternative splicing events were observed including mutually exclusive exons, alternative splice site usage, and exon skipping (Figure 4C; Supplemental Figure S4C; Supplemental Tables S2 and S3). Our RNA sequencing data confirm *TUBG1* and *PCNT* require SON for correct splicing (Supplemental Figure S4C) and identify *CNTROB* and *CEP131* as additional targets that could impact centriole assembly. Therefore, the SON splicing factor is required for the homeostatic control of mRNAs encoding centrosomal, centriolar satellite, and MT cytoskeletal proteins.

SON depletion reduces centriolar satellites and trafficking structures

We examined the distributions of centrosomal and centriolar satellite proteins whose splicing is affected by SON using a semiautomated radial intensity analysis algorithm in control and SON knockdown cells (Figure 5, A and B) (Sankaran *et al.*, 2020). γ-Tubulin, together with γ-tubulin complex members, acts to nucleate MTs and is concentrated at the centrosome (Stearns *et al.*, 1991; Tovey and Conduit, 2018). Utilizing the radial analysis method, SON depletion did not alter γ-tubulin fluorescence intensity at the centrosome itself (the difference from Figure 1 is due to the concentric circle measurements that increase in radius by 0.13 μm as compared with the total fluorescence intensity measured within a 1-μm radius circle). However, the most significant reduction in γ-tubulin was observed in the region 1.0 to 2.5 μm from the centrosome. SON knockdown had a similar effect on the distribution of PCNT, a large scaffolding protein that interacts with γ-tubulin (Dictenberg *et al.*, 1998) and localizes both to the centrosome and to mobile cytoplasmic granules that transit to and from the centrosome (Young *et al.*, 2000; Galati *et al.*, 2018). The PCNT in cytoplasmic granules is nearly eliminated, suggesting that PCNT-dependent trafficking to and from centrosomes is severely affected when SON is depleted (Figure 5, A and B).

Centrobin is associated with daughter centrioles and important for their elongation (Zou *et al.*, 2005; Gudi *et al.*, 2011). Centrobin also limits the recruitment of additional PCM proteins (Jeffery *et al.*, 2013), stabilizes CPAP (Gudi *et al.*, 2014, 2015), and promotes C-tubule formation and maintenance (Reina *et al.*, 2018). This makes centrobin an intriguing candidate for the SON knockdown centriole assembly phenotype as cells with reduced SON initiate but do not complete centriole assembly (Figure 3, A and B), have a larger decrease in centrosomal CPAP than other early centriole assembly factors (Figure 2B), and produce procentrioles without the C-tubule (Figure 3B). We observed that centrobin fluorescence intensity is reduced by 50% at the centrosome with a more severe depletion in the region 1.0 to 1.5 μm from the centrosome in the SON knockdown (Figure 5, A and B).

CEP131 is an integral component of centriolar satellites and important for cilia formation and genomic stability (Graser *et al.*, 2007; Staples *et al.*, 2012; Denu *et al.*, 2019). CEP131 has a significant reduction both near the centrosome and in the region surrounding the centrosome on SON depletion. Measuring total fluorescence within a 5 μm radius around the centrosome shows reductions to the mean of 51, 41, 33, and 16% of control levels for γ-tubulin, centrobin, PCNT, and CEP131, respectively (Figure 5E). Together, these data demonstrate a profound change to the distribution of centrosomal and centriolar satellite proteins in the region surrounding the centrosome.

To understand which changes to protein levels might explain the centriole assembly defect in SON knockdown, we next measured the fluorescence levels of centrosome-localized γ-tubulin, centrobin, PCNT, and CEP131 relative to the frequency of centriole assembly. Correlating fluorescence at and around the centrosome with centriole counts suggested that γ-tubulin levels at and near the centrosome do not explain the SON depletion centriole assembly defect because individual cells with γ-tubulin at levels similar to control cells do not have more centrioles. Importantly, centrobin, PCNT, and CEP131 were reduced to levels in SON knockdown that could contribute to the centriole assembly phenotype (Supplemental Figure S5B).

Because reduction of CEP131 and PCNT demonstrates changes to the trafficking structures and centriolar satellites around the centrosome, we investigated centriolar satellites further. We examined localization of the canonical centriolar satellite scaffold protein, PCM1, in the SON knockdown even though siSON's effect on *PCM1* mRNA expression was modest (85% of control). PCM1 and CEP131 are both major centriolar satellite proteins with considerable overlap in their localization at centriolar satellites (Kubo *et al.*, 1999; Dammermann and Merdes, 2002; Staples *et al.*, 2012; Gheiratmand *et al.*, 2019; Prosser and Pelletier, 2020). Similar to CEP131, PCM1 fluorescence intensity was reduced throughout the radial analysis, although not to the same degree (34% of control vs. 16% for CEP131) (Figure 5, C–E, and Supplemental Figure S5, A and B). Taken together, this indicates that SON is required for the proper levels and distribution of centriolar satellites.

To assess whether the reduction in centriolar satellite fluorescence intensities at or around the centrosomes was due to mislocalization or total cellular loss of protein, total fluorescence levels inside cells were quantified in both siSON and siControl cells (Figure 5F). Some proteins whose genes depend on SON for correct splicing had significant reductions in overall protein levels (83% for γ-tubulin, 53% for PCNT, and 44% for CEP131). PCM1 was also reduced in total protein levels (78%) despite proper splicing during SON depletion, suggesting that when satellites are disrupted, PCM1 protein stability is affected. We also detected an elevation in total cellular SAS-6 protein levels, even though there was not a large transcriptional change as determined by RNA-sequencing (1.06-fold change relative to siControl). In summary, SON activity is required for the normal accumulation and distribution of centriolar satellites and PCNT trafficking structures. It may do so through its robust effect on CEP131 protein levels.

SIM imaging revealed localization of PCM1 and CEP131 directly adjacent to nascent procentrioles in siControl cells (Figure 5, A and C). This localization, as well as the formation of GFP–centrin-positive procentrioles, is ablated when SON is depleted. This suggests that centriolar satellites (which are also important for centrin accumulation at centrosomes; Dammermann and Merdes, 2002) and trafficking
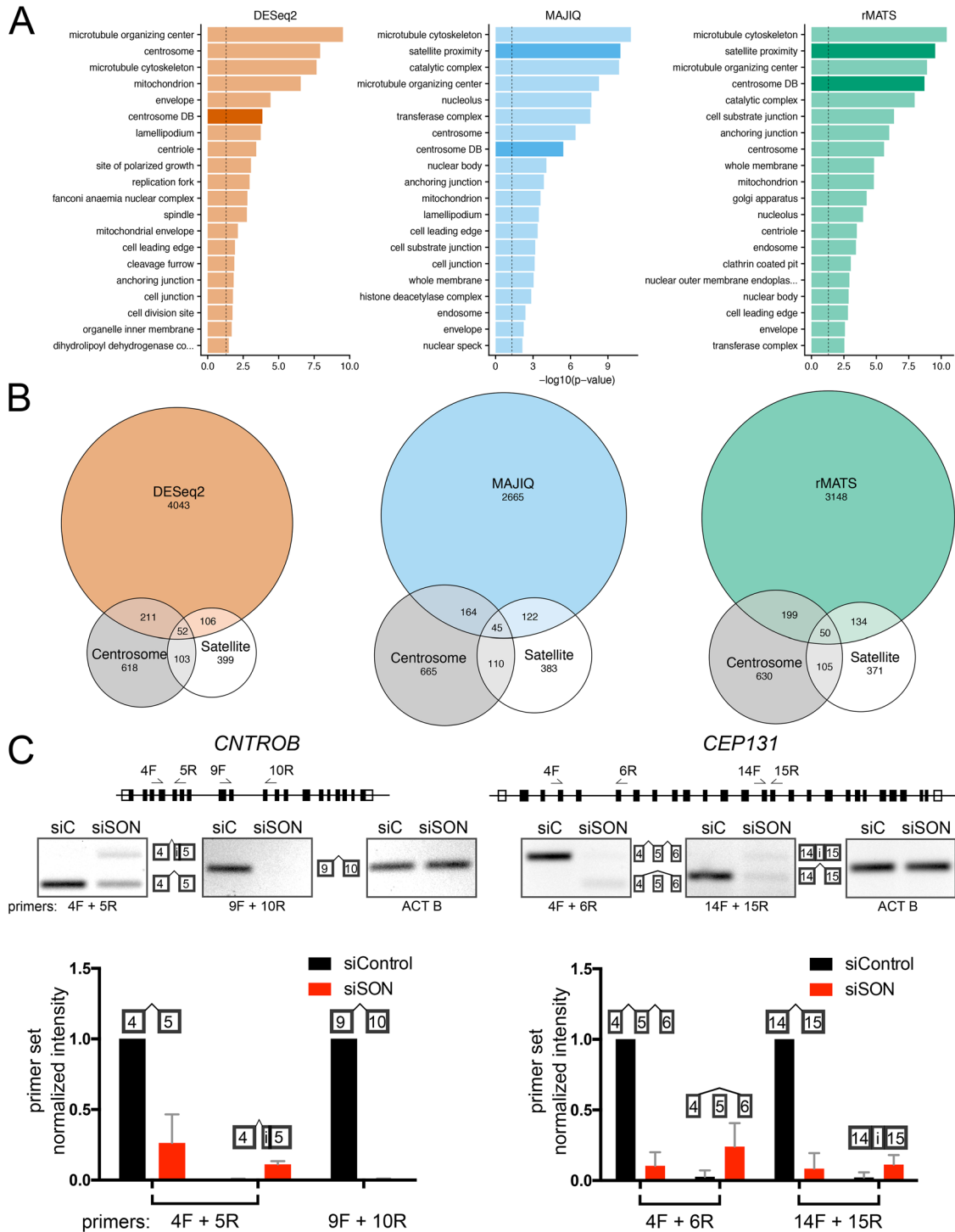
FIGURE 4: SON depletion disrupts splicing of genes responsible for centriole assembly, centriolar satellites, and the MT cytoskeleton. (A) The centrosome fraction of the CCDB, centrosome DB (Gupta *et al.*, 2015), and genes determined by proximity mapping of centriolar satellites (satellite proximity) (Gheiratmand *et al.*, 2019) was included with GO terms in opaque colors. The top 20 terms for reduced gene expression (DESeq2) and alternative splicing (as determined by either the MAJIQ or rMATS software packages) are ordered by *p* values. The dashed lines indicate a *p* value of 0.05. (B) Venn diagrams displaying the overlap of the CD (Centrosome), the centriolar satellite proximity list (Satellite) and reduced expression or spliced genes. Areas of each circle are proportionate with the gene set. (C) SON depletion results in improper splicing of *CNTROB* and *CEP131*. Top panels show the location of introns and exons and the primers used for reverse transcriptase PCR (RT-PCR), middle panel. Bottom panel: quantification of the RT-PCR bands normalized first to the amount of RNA as determined by ACT B RT-PCR and second to the amount of the properly spliced fragment in the control condition. RNA-seq and RT-PCR were performed and quantified on three biological replicates. Error bars: SD.
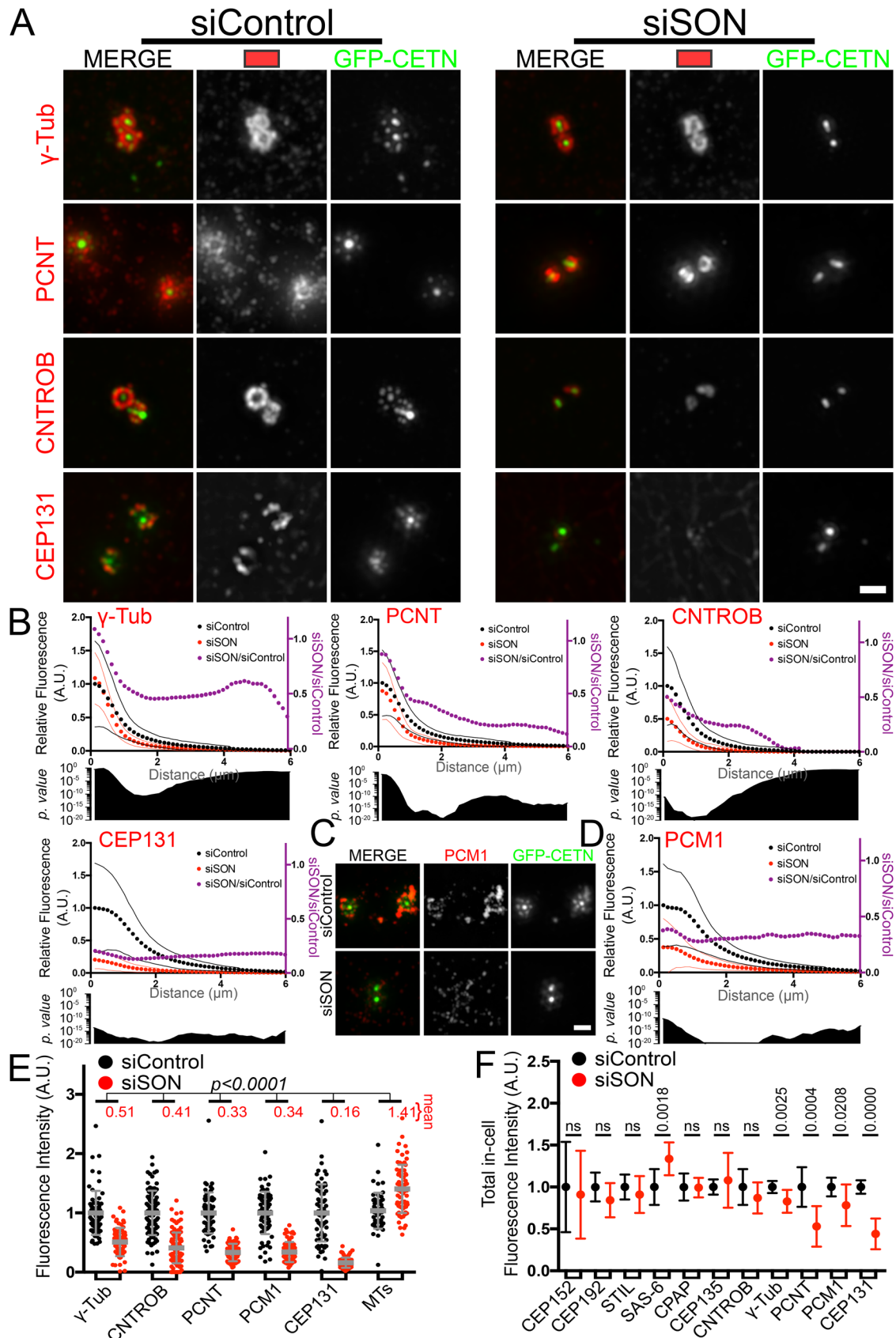
FIGURE 5: SON splicing targets disrupt centrobin, centriolar satellites, and trafficking granules. (A) SON targets are diminished at the centrosome. SIM images of siRNA-treated, S phase-arrested cells induced for PLK4 expression and stained for the identified SON targets. Scale bar = 1 μm. (B) γ-Tsubulin and PCNT are reduced most in the region 1.0 to 2.5 μm from the centrosome center. Normalized mean radial quantification of fluorescence intensities from widefield

particles participate in late steps of centriole assembly and are affected by SON. This relationship between satellites and newly assembling centrioles is also observed in S phase-arrested cells without PLK4 induction (Supplemental Figure S1D).

SON depletion alters the MT landscape near the centrosome

Because centriolar satellites utilize MT-dependent trafficking (Kubo *et al.*, 1999; Conkar *et al.*, 2019), and because we observed close association between centriolar satellites and the assembling procentrioles, we examined the MT network near centrosomes. We observed a twofold increase in MT density in SON-depleted cells, consistent with previous reports (Figures 5E and 6, A and B; Supplemental Figure S5, A and B) (Ahn *et al.*, 2011). Using SIM, we resolved the relationship between assembling centrioles, MTs, and centriolar satellites and observed MTs originating in close proximity to nascent procentrioles (Figure 6C). Furthermore, the centriolar satellite protein, PCM1, is positioned at the ends of these MTs, suggesting that assembling centrioles utilizes MTs and centriolar satellites for delivery of components required for their elongation and maturation. When SON is depleted, the MT arrangement is distinctly different, with MTs crowded around mother centrioles. To quantify this rearrangement, we examined the MT intensity around mother centrioles to determine the average distance at which MTs begin. Because the average intensity of MTs dissipates as a function of distance from the centrosome (Figure 6B), we examined the shift from increasing MT intensity to decreasing intensity as measurements are quantified radially from the mother centriole as a way to establish the boundary of MT minus ends close to the centrosome. This occurred on average 480 nm from the mother centrioles in siControl cells and 340 nm in siSON cells (Figure 6, C and D), indicating that not only are there more MTs around centrosomes when SON is depleted but that the network encroaches closer to the mother centrioles.

We next analyzed the relationship between MT minus ends and centrioles in electron microscopy (EM) tomograms. Consistent with the fluorescent image analysis, MTs on average originated closer to the mother centriole on SON depletion (408 nm) as compared with control conditions (483 nm) (Figure 6, E and F; Supplemental Figure S6, A and B). Although centriolar satellites are difficult to discern without a protein marker (Kubo *et al.*, 1999), the cytoplasmic content in SON-depleted cells is markedly different from that of control cells with a dramatic increase in the number of vesicles present near the centrosome (see Supplemental Movies S2 and S4–S7).

To explore how SON influences the MT network organized by centrosomes, we examined the localization of the p80 subunit of the Katanin complex responsible for its centrosomal localization (McNally *et al.*, 2000). Katanin p80 is encoded by *KATNB1* whose mRNA splicing is affected by SON (Supplemental Figure S4C) (Ahn *et al.*, 2011). Furthermore, the absence of Katanin p80 stabilizes MTs near the centrosome (Hu *et al.*, 2014). *KATNB1* mRNA abundance is reduced in siSON to 18% of the siControl samples (Supplemental Table S1), and splicing efficiency is also reduced, particularly at the 3′ end of the gene (Supplemental Figure S4C). Katanin p80 localization can sometimes be discerned around the interphase centrosome in the region between the mother centriole and the procentrioles. This localization is reduced when SON is depleted (Figure 6, G and H). This raises the possibility that MTs are remodeled by centrosome-localized Katanin to facilitate a transition from the mother centriole to nascent procentrioles for daughter centriole elongation and assembly.

Depletion of specific SON-spliced genes does not fully recapitulate the centriole assembly defects observed in SON knockdown.

To assess the contributions of the SON targets centrobin, CEP131, PCNT, and Katanin p80 to the centriole assembly defect observed in SON depletion, we evaluated centriole assembly upon knockdown of these individual components. Knockdowns of *CNTROB* and *CEP131* mRNAs effectively reduced the corresponding proteins at centrosomes in the PLK4 overexpression cells after 48 h (Figure 7, A and B). However, centriole assembly was only modestly affected on knockdown of centrobin or CEP131 individually or in combination (Figure 7C), indicating that depletion of these proteins, on their own, do not account for the reduction in centriole assembly observed with SON knockdown. Because centrobin has been reported to stabilize CPAP (Gudi *et al.*, 2014, 2015), we examined whether centrobin knockdown would recapitulate the reduction in CPAP observed when SON is depleted (Figure 2B). Surprisingly, centrobin depletion resulted in a modest increase to CPAP fluorescence intensities at centrosomes in the PLK4 induction experiments (Supplemental Figure S7, A and B). Therefore, changes to centrobin levels as a result of SON depletion are unlikely to contribute to the reduced CPAP levels and centriole assembly observed in the SON knockdown.

Because centrobin had a modest effect on centriole assembly, we focused on the effects of CEP131 and PCNT. Localization of PCM1 in both SON depletion and CEP131 depletion was reduced

images (Supplemental Figure S5A) (y-axis on the left, black = siControl, red = siSON). The ratio of the intensity of siSON/siControl is also plotted (y-axis on the right, purple); p values from the Student's t test are plotted beneath each graph on a semilog scale. The mean value is plotted, and standard deviations are plotted as thin lines in the corresponding color. N = γ-tubulin: siControl, 76 centrosomes; siSON, 73 centrosomes; PCNT: siControl, 72 centrosomes; siSON 76 centrosomes; centrobin (CNTROB): siControl, 101 centrosomes; siSON, 106 centrosomes; CEP131: siControl, 70 centrosomes; siSON, 96 centrosomes. Data are compiled from two biological replicates. (C) SIM images of siRNA-treated, S phase-arrested cells induced for PLK4 expression and stained for PCM1. Scale bar = 1 μm. (D) Radial quantification of PCM1 fluorescence intensity as in B. N = siControl, 78 centrosomes; siSON, 70 centrosomes. Data are compiled from two biological replicates. (E) Fluorescence quantification of the indicated proteins in a 5-μm radius circle around the centrosomes. N = γ-tubulin: siControl, 65 cells; siSON, 63 cells; centrobin (CNTROB): siControl, 90 cells; siSON 100 cells; PCNT: siControl, 65 cells; siSON, 66 cells; PCM1: siControl, 74 cells; siSON, 67 cells; Cep131: siControl, 66 cells; siSON, 73 cells; MTs: siControl, 55 cells; siSON 68 cells. Bar and error bars: mean and SD. Data are compiled from two biological replicates. (F) Total mean in cell fluorescence intensities. Fluorescence was measured simultaneously for all cells in each image, and 10 images total were used for each marker except for CEP131, where nine images were used, and centrobin (CNTROB), where 16 images were used. Data are compiled from two biological replicates. Bars and error bars: mean and SD; ns, not significant.
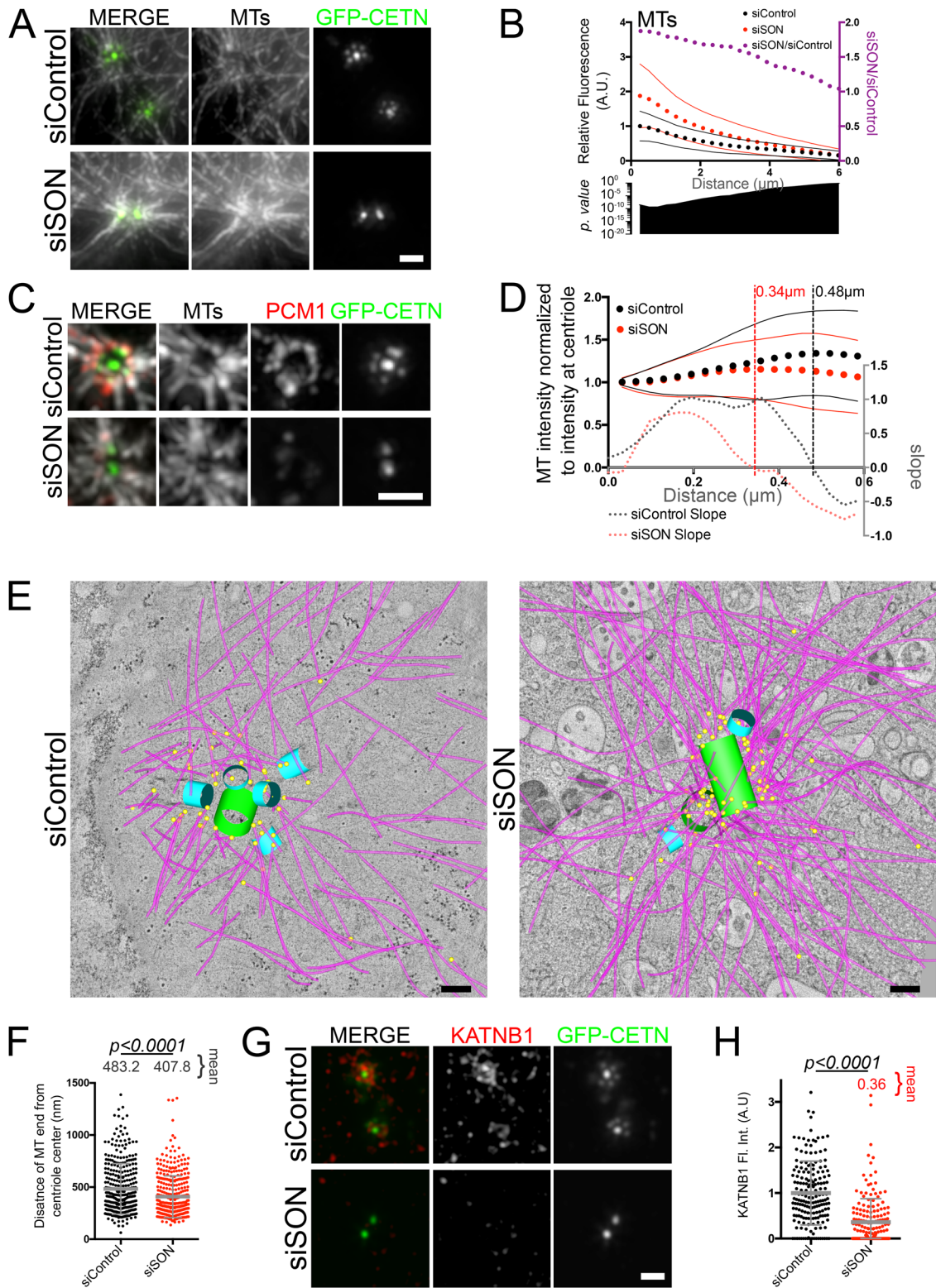
FIGURE 6: SON depletion increases the density of centrosomal MTs from the mother centriole and reduces Katanin at the centrosome. (A) The density of MTs around the centrosome is increased when SON is depleted. SIM images of siRNA-treated, S phase-arrested cells induced for PLK4 expression and stained for MTs (gray). (B) Radial quantification of MT fluorescence intensities from the centrosome (y-axis on the left, black = siControl, red = siSON). The ratio of the intensity of siSON/siControl is also plotted (y-axis on the right, purple). The p values from the Student's t test are plotted beneath each graph on a semilog scale. N = siControl: 46 cells; siSON: 63 cells from two biological replicates. (C) Procentriole, centriolar satellite, and MT colocalization is disrupted by SON depletion. SIM images of siRNA-treated, S phase-arrested cells induced for PLK4 expression and stained for PCM1 (red) and MTs (gray). (D) MTs originate closer to the mother centriole in SON-depleted cells. MT fluorescence intensities from line scans of SIM images of 10 mother

to similar levels (Figure 7, D and E), indicating that the PCM1 reduction observed with SON depletion can be attributed to the reduction in CEP131. CEP131 has also been implicated in the trafficking of CEP152 to the centrosome (Kodani *et al.*, 2015; Denu *et al.*, 2019). To assess whether the centrosomal CEP152 reduction observed with SON depletion is due to loss of CEP131, we quantified centrosomal CEP152 fluorescence in both SON and CEP131 depletion conditions. Reductions in CEP152 were observed in both conditions (Supplemental Figure S7, C and D). Treatment with siCEP131 was more effective at reducing CEP131 levels than treatment with siSON, but CEP152 levels in siSON were reduced by slightly more than by siCEP131 alone. This suggests that promotion of correct *CEP131* splicing by SON is partially responsible for the observed reduction in CEP152.

We next examined how PCNT depletion in siSON contributes to the centriole assembly defect. Depletion of PCNT was efficient and reduced centriole assembly to a greater degree than depletion of CEP131, although not to the level of SON depletion (Figure 7, F–H). Depletion of both CEP131 and PCNT concurrently had a similar effect on centriole assembly as depletion of PCNT alone (Figure 7H). SON depletion, interestingly, reduces PCNT at the mother centrioles to 60–80% of controls (Figures 5, A and B, and 7, F and I), whereas PCNT depletion reduces this population to 15% (Figure 7, F and I), making the contribution of SON-dependent splicing of PCNT to the centriole assembly defect difficult to assess (Figure 7, F and I). However, it raises the possibility that alternative splicing controlled by SON is specifically necessary for the trafficking population of PCNT (Figure 5, A and B). Indeed, four distinct exon skipping events in *PCNT* were detected by the rMATS method (Supplemental Table S3). The most prevalent introduces a premature stop codon, while the other three leave the majority of the protein in frame and maintain the C-terminal PACT domain, which is required for the centriolar localization of PCNT (Gillingham and Munro, 2000). Additionally, we examined the interplay between CEP131 and PCNT. Consistent with previous reports (Staples *et al.*, 2012), CEP131 depletion results in a modest decrease in PCNT fluorescence intensity around the centrosome (56%), while PCNT depletion causes a dramatic decrease in CEP131 fluorescence intensity around the centrosome (18%) (Figure 7, G and I). Therefore, reductions in the SON splicing targets CEP131 and PCNT account for the loss of centriolar satellites observed in cells depleted of SON, but do not fully account for the SON depletion centriolar assembly defect.

Because SON depletion is permissive for early steps of centriole assembly but prevents advancement of the assembly process, we examined CEP131 and PCNT depletion for procentriole intermediates as found in the SON knockdown. We utilized SAS-6 fluorescence as a proxy for these procentriole intermediates. In SON-depleted cells, we once again observed SAS-6 signal in a rosette

formation without centrin foci. Early centriole assembly intermediates were never observed when PCNT was depleted, which is consistent with reports that SAS-6 requires PCNT for its localization (Ito *et al.*, 2019) and only rarely observed when CEP131 was depleted (Supplemental Figure S7, E–G). We therefore conclude that when SAS-6 is present at procentrioles in PCNT-depleted cells, centriole assembly is able to proceed. When SAS-6 is present at procentrioles in CEP131-depleted cells, centriole assembly usually proceeds, but occasionally is slowed or arrested, as is the case for most cells depleted of SON (Supplemental Figure S7G). This indicates that the trafficking particles supported by CEP131 and SON are important for procentriole elongation and centrin deposition.

Because we observed a reorganized MT network around centrosomes on SON depletion, we examined whether the katanin MT-severing complex contributes to this alteration and whether it functions to facilitate procentriole assembly. Katanin p80 reduction resulted in a slight reduction to centriole assembly, but very little change to the overall distributions of MTs and PCM1 (Figure 7, J–L), suggesting that reduction of Katanin p80 is not responsible for the gross MT changes observed when SON is depleted. Neither did depletion of Katanin p80 phenocopy the origination of MTs nearer to the mother centriole that is observed with SON depletion (Supplemental Figure S7I). Therefore, the major changes to the interphase MT network upon SON depletion are not primarily due to the SON-dependent reduction of Katanin p80.

In total, CEP131 and PCNT depletion can recapitulate some of the centriole assembly defects observed when SON is depleted, but neither depletion of these proteins individually or in combination nor depletion of centrobin or Katanin p80 can explain the severe centriole assembly defect observed upon SON depletion. This suggests that the mechanism of SON-based regulation of centriole assembly is multifactorial and may be dependent on specific splice isoforms rather than simple depletion of centriole assembly and centrosome trafficking proteins.

SON facilitates cilium assembly

Because SON depletion results in a dramatic reduction of centriolar satellites, and because centriolar satellites are required for efficient cilium assembly (Odabasi *et al.*, 2019), we examined primary ciliogenesis upon SON depletion (Supplemental Figure S8A shows SON knockdown under these conditions). After 42 h of serum starvation, 50% of siControl-treated cells formed a cilium. In contrast, only 18% of siSON-treated cells were able to do so (Figure 8, A and B). To assess whether this was due to a deficiency in the mother centriole, we assessed the presence of the distal appendage protein, CEP164 (Graser *et al.*, 2007; Yang *et al.*, 2018) and found it is at mature centrioles at a frequency identical to controls (Figure 8, A and C). Furthermore, distal and subdistal appendages were

centrioles (five cells) for both siControl and siSON (*y*-axis on the left, black = siControl, red = siSON). Intensities were normalized to the signal at the center of each individual centriole and lines were rotated at 45° intervals (eight measurements per centriole). The mean of all line scans is plotted along with the SD. The slope of these lines is plotted (*y*-axis on the right) and the vertical lines indicate where the fluorescence intensity begins to decrease in each condition. (E) MTs emanate primarily from the mother centriole when SON is depleted. Tomographic slices with modeled centrioles (green), procentrioles (blue), and MTs (magenta) overlayed. (F) Distances of the MT minus ends to the center of the centriole. *N* = siControl, 340 MTs; siSON, 379 MTs from four and five tomographic models, respectively. (G) Katanin localization around the mother centriole is dependent on SON. SIM images of siRNA-treated S phase-arrested cells induced for PLK4 expression stained for Katanin p80 (KATNB1) (red). (H) Fluorescence quantification of Katanin p80 (KATNB1) in a 1-μm radius circle around the centrosome from widefield images. *N* = siControl: 184 centrosomes; siSON 177 centrosomes from three biological replicates. Scale bars = 1 μm for A, C, and G. Scale bars = 200 nm in E. Bar and error bars: mean and SD.
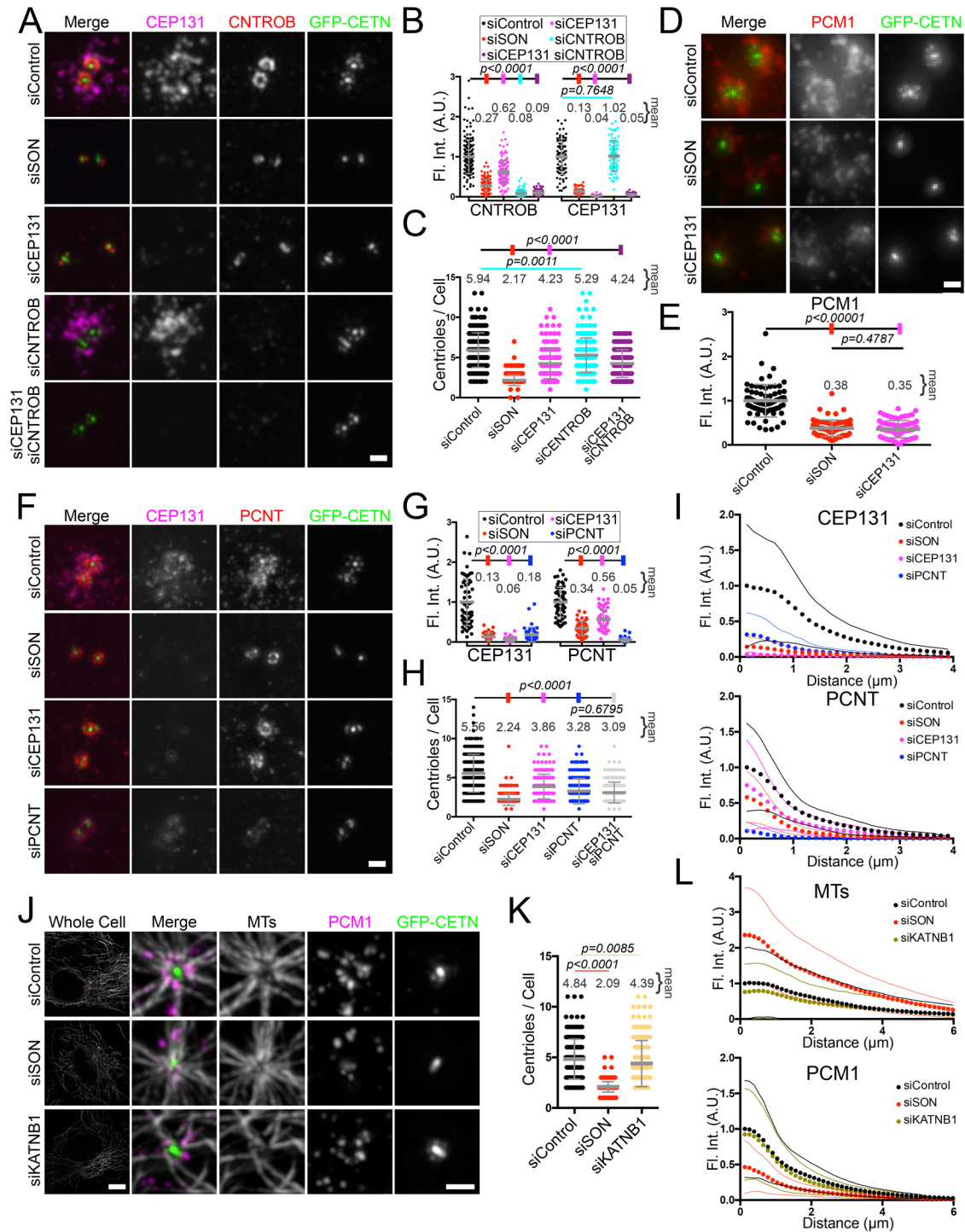
FIGURE 7: Depletion of SON splicing targets partially phenocopy SON depletion. (A) *CEP131* knockdown partially inhibits centriole assembly. SIM images of CEP131 and centrobin (CNTROB) stained cells depleted of SON, CEP131, centrobin, or both CEP131 and centrobin. (B) Fluorescence quantification of widefield images of CEP131 (5-μm radius— cell) and centrobin (1-μm radius—centrosome). *N* = siControl: 165 centrosomes, 85 cells; siSON: 158 centrosomes, 78 cells; siCEP131: 151 centrosomes, 71 cells; siCNTROB: 161 centrosomes, 81 cells; siCEP131 and siCNTROB: 173 centrosomes, 86 cells. (C) Centriole counts after S phase arrest and PLK4 induction in indicated siRNA conditions. *N* = 180 cells for each condition. Quantifications are from two biological replicates. (D) Depletion of CEP131 results in a reduction in PCM1 around the centrosome. Widefield images of cells stained for PCM1 after SON or CEP131 depletion and S phase arrest and PLK4 induction. (E) PCM1 fluorescence quantification of a 5-μm radius circle around centrosomes in images from D. *N* = siControl: 67 cells; siSON: 68 cells; siCEP131: 75 cells. Quantifications are from two biological replicates. (F) PCNT depletion reduces centriole assembly and CEP131 localization. SIM images of S phase-arrested and PLK4-induced cells stained for CEP131 and PCNT. SON, CEP131, and PCNT were depleted as indicated. (G) Fluorescence quantification of widefield images of CEP131 and PCNT within a 5-μm radius around the centrosomes.
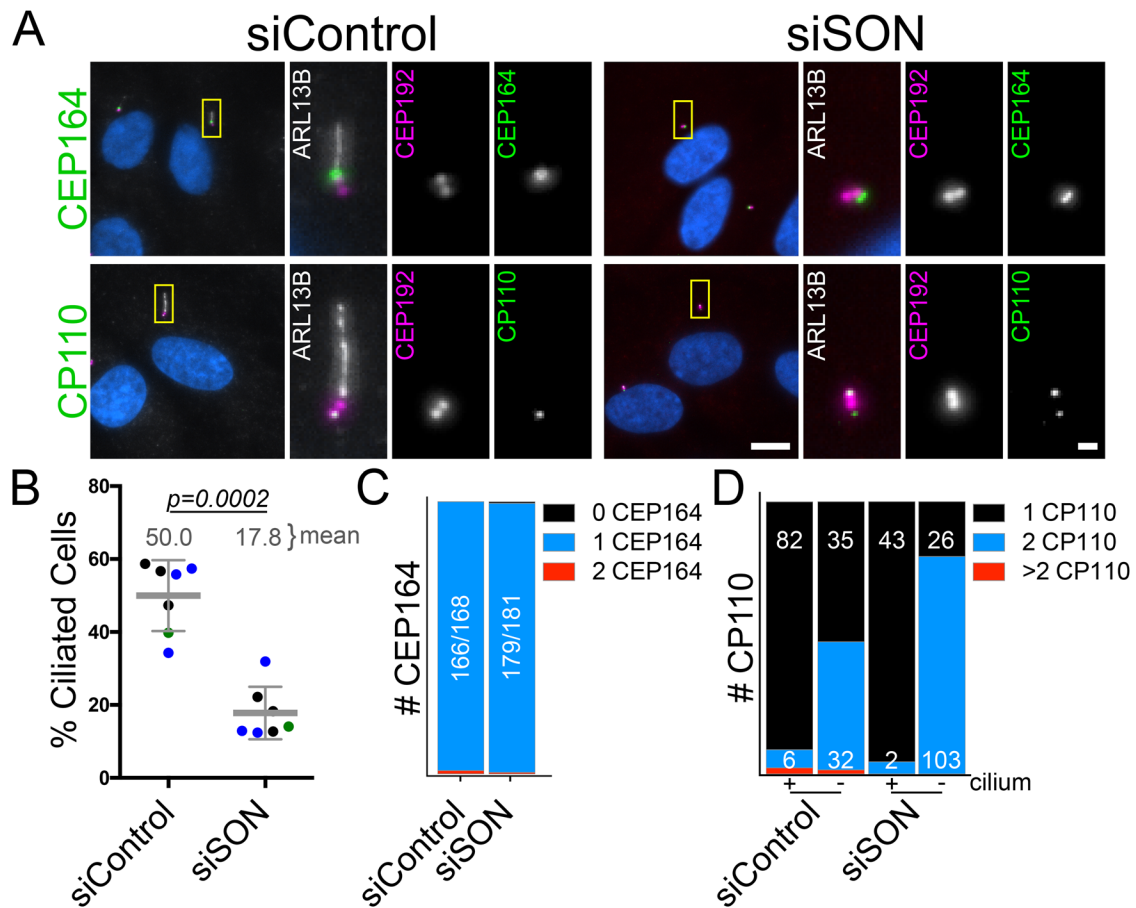
FIGURE 8: SON facilitates cilium assembly. (A) Widefield images of serum-starved RPE-1 cells stained with ARL13B for cilia, CEP192 for centrioles, and CEP164 or CP110. (B) Percentages of cells with cilia. Three biological replicates are represented by different colors (black, blue, and green). Each dot represents a technical replicate. (C) The number of CEP164-spositive centrioles per cell. (D) The number of CP110 positive centrioles per cell. Cells are separated by their cilium status. Number of cells are indicated within the bars and are from two biological replicates. Bar and error bars: mean and SD.

observed in EM tomograms (Supplemental Figure S6A; Supplemental Movie S4), suggesting that SON depletion does not result in the loss of these centriolar structures required for ciliogenesis. Ciliogenesis is inhibited by the presence of a CP110 cap that is removed prior to cilia assembly (Spektor *et al.*, 2007; Chen *et al.*, 2021); 80% of SON-depleted cells without cilia have two discernable CP110 foci while 95% of SON-depleted ciliated cells have one, indicating that the reduction in ciliogenesis is due to a defect after centriole maturation leading up to CP110 removal. Trafficking of preciliary vesicles precedes CP110 removal and utilizes MT and actin-dependent trafficking (Lee *et al.*, 2017; Wu *et al.*, 2018). Given that trafficking

structures are disrupted in SON depletion, it is notable that SON-depleted cells with cilia have slightly higher amounts of PCNT and CEP131 than SON-depleted cells without cilia (Supplemental Figure S8, B and C). This suggests that disrupted centrosomal trafficking as a result of SON depletion reduces ciliogenesis.

DISCUSSION
We have shown that the function of the splicing factor SON is required for centriole assembly, independent of its effects on the cell cycle. Although centriole assembly initiates in the absence of SON, procentrioles do not form completely. Correct splicing of the gene

---

encoding the centriole assembly factor centrobin, which is required for centriole elongation, is dependent on SON activity. The absence of centrobin does not explain the absence of centrin incorporation (a marker of more mature procentrioles) observed with SON depletion but may contribute to the lack of triplet MTs in the procentrioles. SON is also responsible for promoting proper mRNA splicing of *CEP131*, which encodes a core centriolar satellite protein. SON depletion profoundly disrupts the distribution of centriolar satellites and PCNT trafficking granules around the centrosome. Yet even the depletion of CEP131 and PCNT alone or in combination cannot fully recapitulate the centriole assembly defect caused by loss of SON. SON also affects the splicing of *KATNB1*, which encodes for the p80 centrosomal targeting subunit of katanin. Katanin p80 depletion, however, cannot explain the increase in MT density near centrosomes in SON depletion cells. Depletion of these factors does not replicate the SON depletion centriole assembly phenotype, leaving open a number of possibilities as to how SON controls this process. One is simply that we did not identify the critical SON targets responsible for centriole assembly. A second possibility is that splice isoforms generated by SON have specific repressive effects on centriole assembly as is the case for the short isoform of CEP135 (Dahl *et al.*, 2015). This would not be replicated by simple RNAi depletions. Together, these data suggest that SON has an important role in controlling factors critical for trafficking particles around the centrosome and the MT cytoskeletal network on which they rely.

Whether centriolar satellites are required for centriole assembly appears to be cell type dependent as different centriole assembly responses to centriolar satellite disruption are observed. Cell lines developed from cancer cells (HeLa, U2OS) utilize centriolar satellite transport for centriole assembly, whereas hTERT immortalized cells (RPE-1) forgo this pathway (Hori *et al.*, 2015; Kodani *et al.*, 2015). In this study, using RPE-1 cells, we observed a close association of centriolar satellites with assembling procentrioles, but depletion of satellites (through CEP131 depletion) and PCNT-associated trafficking particles caused reductions in centriole assembly, but did not eliminate it. The resilience in centriole assembly observed in this study could be due to the S phase arrest and PLK4 induction used in these experiments, which may make the process unnaturally robust. Alternatively, it could reflect the lack of reliance on centriolar satellites for centriole assembly in RPE-1 cells.

There is, however, increasingly strong evidence that centriolar satellites are required for primary cilia formation and function (Chamling *et al.*, 2014; Kurtulmus *et al.*, 2015; Hori *et al.*, 2016; Odabasi *et al.*, 2019). Indeed, we found that SON depletion is deleterious to cilia formation. This is consistent with the discovery that *de novo* mutations in *SON* are associated with intellectual disabilities (Kim *et al.*, 2016; Tokita *et al.*, 2016), which can be caused by ciliary defects (Youn and Han, 2018). *SON* resides on human chromosome 21 and is therefore one of the genes whose dosage is altered in Down syndrome. Given that individuals with Down syndrome have defects in their cilia and cilia-dependent signaling (Roper *et al.*, 2006; Moldrich *et al.*, 2007; Galati *et al.*, 2018), the role that *SON* dosage plays in cilia formation and function requires investigation.

SON's activities could be required constitutively or modulated for unique cell cycle and developmental programs. Our data indicate that SON can effectively control centrosome assembly, which would have consequences for both the cell cycle and development. SON was identified to be important for maintaining human embryonic stem cell (hESC) identity (Chia *et al.*, 2010), and its depletion led to hESC differentiation into a fibroblastlike state with a consequent down-regulation of pluripotency-associated genes, up-regulation of differentiation-associated genes, and no change to housekeeping genes (Lu *et al.*, 2013). In support of SON regulation contributing to control of developmental programs, SON is necessary for full telomerase activity in hESCs by its promotion of exon-2 retention in the hTERT transcript (Penev *et al.*, 2021). As pluripotency requires high-fidelity cell divisions and centrosomes, SON control of centrosome assembly could contribute to stemness and provide a powerful avenue to regulate both cell division during differentiation and centrosomal function as a dominant MTOC in cell types that utilize noncentrosomal MTOCs in their differentiated state.

In conclusion, SON activity has a strong positive impact on trafficking particles around the centrosome, including centriolar satellites and cytoplasmic PCNT granules, and plays an important role in completing procentriole assembly. SON is required for the correct mRNA splicing of *CEP131* and the efficient splicing of *PCNT*. SON is also involved in the remodeling of the underlying MT network on which centriolar satellites and PCNT trafficking particles rely. In addition, SON is important for proper splicing of *CNTROB*, the gene encoding centrobin which is important for centriole elongation and MT triplet formation. Together, SON acts as a critical nexus for a powerful, multifactorial control of centriole assembly through its influence on genes required for the MT network and centriolar satellites that support centriole assembly and ciliogenesis.

Data availability
Raw and processed RNA sequencing data for this study have been deposited at NCBI GEO under accession number GSE164278.

MATERIALS AND METHODS
Request a protocol through *Bio-protocol*.

Cell culture growth conditions and small interfering RNA treatments
RPE-1/Tet-PLK4 GFP-CETN (the kind gift of M.B. Tsou) (Hatch *et al.*, 2010) were grown in DMEM/high glucose with glutamine (Cytiva or Life Technologies) with 10% tetracycline-free fetal bovine serum (FBS; Peak Serum) supplemented with penicillin and streptavidin (Life Technologies) at 37°C with 5% CO_2. For PLK4 induction experiments, cells were plated onto 12-mm circular cover glass, No. 1.5 (Electron Microscopy Sciences) coated with collagen (Sigma, C9791) in 24-well plates at 11,000 to 12,500 cells per well. The following day, cells were treated with small interfering RNAs using the Lipofectamine RNAiMAX Transfection Reagent (Thermo Fisher Scientific) following the manufacturer's instructions. Transfection complexes were removed from cells after 5 h; 24 h after transfection complexes were added, cells were arrested with 1.6 µg/ml aphidicolin (Cayman Chemical Company). PLK4 was induced with 1 µg/ml doxycycline (Sigma-Aldrich) 7 h after aphidicolin arrest was initiated. Cells were fixed 17 h after PLK4 induction.

Ciliogenesis experiments were conducted in RPE-1 cells (ATCC) grown in DMEM/F12 (Cytiva) with 10% FBS (Peak Serum). Cells were plated at 45,000 cells per coverslip and treated with siRNAs the following day. After 5 h of treatment with siRNAs, complexes were removed and replaced with fresh medium containing 0.5% FBS. Cells were fixed 48 h after the initiation of siRNA treatment.

siRNAs utilized were siControl: Mission siRNA Universal Negative Control #1 SIC001 (Sigma Aldrich), SON: Stealth P5A8 (all experiments), GCGCUCUAUGAUGUCAGCUUAUGAA; Stealth P5A7, CC-GAUCUAUGAUGUCAUCUUAUACU; CEP131: Stealth HSS146116, CAGAGUGCCAGGAAUGCGGCAGCCU; CNTROB: Silencer Select s42058 GCAUUGGAUUCAGAGCAUAUt; KATNB1: Silencer Select s20140, GAACAUCGUCAACCAGAAAtt (used in all KATNB1 knockdown experiments and identified as siKATNB1 1 in Supplemental

Figure S7H) and Silencer Select s20141, GCAGAUGACCACACC-GUGAtt (identified as siKATNB1 2 in Supplemental Figure S7H). Stealth siRNAs were used at 50 nM, and Silencer Select siRNAs were used at 10 nM (Thermo Fisher Scientific). PCNT was targeted with an siGenome Smartpool (Dharmacon) at 5 nM. The Mission Universal Negative siRNA was used at 50 nM.

A PCR test was used to check for mycoplasma contamination once every 6 mo.

Immunofluorescence
Cells were fixed in cold MeOH for 8 min, washed three times in phosphate-buffered saline (PBS), and blocked in Knudsen buffer (1× PBS, 0.5% bovine serum albumin, 0.5% NP-40, 1 mM $MgCl_2$, 1 mM NaN_3) for 1 h. Cells stained for tubulin were fixed with glutaraldehyde and formaldehyde as previously described (Canman et al., 2000). Antibody staining was conducted at room temperature for 1 to 2 h. Samples were washed 3 times for 5 min in PBS prior to secondary antibody and DNA staining in Knudson buffer for 1 h, except for samples stained for tubulin in which fixes, staining, and washes were conducted in PHEM buffer. Primary antibodies: 1:500 α-ARL13B (Antibodies Incorporated N295B/66); 1:1000 α-centrobin (Proteintech 26880-1-AP); 1:10,000 α-CEP131 (the generous gift of J. Reiter, Department of Biochemistry and Biophysics, University of California, San Francisco School of Medicine, San Francisco, CA); 1:300 α-CEP135 (Proteintech 24428-1-AP); 1:2500 α-CEP152 (Bethyl A302-480A); 1:500 α-CEP164 (Protein Tech 22227-1-AP); 1:2000 α-CEP192 (the generous gift of A. Holland, Department of Molecular Biology and Genetics, Johns Hopkins University School of Medicine, Baltimore, MD); 1:500 α-CPAP (Proteintech CENPJ 11517-1-AP); 1:500 α-CP110 (Proteintech 12780-1-AP); 1:200 α-FLAG (Sigma, M2); 1:50 α-KATNB1 (Proteintech 14969-1-AP); 1:2000 α-PCM1 (Bethyl A301-150A); 1:2000 α-PCNT (Abcam ab4448); 1:2000 α-SAS-6 (Bethyl A301-802A); 1:4000 α-SON (Thermo Fisher Scientific PA5-65107); 1:2500 α-STIL (Bethyl SIL A302-441A); 1:300 α-α-tubulin (Sigma DM1A); 1:2000 α-γ-tubulin (Sigma, DQ19). Secondary staining: 1:1000 Alexa anti-rabbit 594, Alexa anti-mouse 594, Alexa anti-guinea pig 647, and Hoechst 33342 (Thermo Fisher Scientific). Coverslips were mounted on Citifluor (Ted Pella) and sealed with clear nail polish.

Fluorescence imaging
Images were collected using a Nikon TiE (Nikon Instruments) inverted microscope stand equipped with a 100× PlanApo DIC, NA 1.4 objective. Images were captured using an Andor iXon EMCCD 888E camera with 0.3-μm Z steps. SIM images were acquired using a Nikon SIM (N-SIM) with a Nikon Ti2 (Nikon Instruments; LU-N3-SIM) microscope equipped with a 100× SR Apo TIRF, NA 1.49 objective. Images were captured using a Hamamatsu ORCA-Flash 4.0 Digital CMOS camera (C13440) with 0.1-μm Z step sizes. Reconstructions were generated with Nikon Elements. All images were collected at 25°C using NIS Elements software (Nikon). Raw SIM images were reconstructed using the image slice reconstruction algorithm (NIS Elements).

Centriole counts
GFP-Cetn fluorescence was utilized to count centrioles manually using the 100× PlanApo DIC, NA 1.4 objective with the optivar in on the Nikon TiE inverted microscope stand, providing 1.5× magnification.

Image analysis
Image analysis was done using Fiji (Schindelin et al., 2012). Image stacks were maximum intensity projected. Fluorescence intensities

of centrosomes were measured within a 1-μm radius circle encompassing each individual centrosome (mother and daughter centrioles). A measurement of in cell intensity near each centrosome was taken for subtraction of noncentrosomal signal. To measure the fluorescence intensity of proteins with satellite and trafficking populations, fluorescence was measured within a 5-μm radius circle encompassing both centrosomes and the surrounding cytoplasm. A similar circle was measured within the cell that did not include the centrosomes to calculate the in-cell background. If subtraction of background signal generated a negative result for fluorescence, it was converted to 0.

For radial fluorescence intensity analyses, we utilized the algorithm described in Sankaran et al. (Sankaran et al., 2020) using the PCM or MT analysis tool. Briefly, maximum intensity-projected images were selected for analysis. Centrosomes and cells identified by the algorithm were manually checked for accuracy prior to the algorithm calculating the in-cell radial fluorescence intensity.

SON total nuclear fluorescence intensity was measured in Fiji by subtracting the average background (calculated from all images analyzed in a 5-μm radius circle outside of the cells) from each image. The DNA signal (Hoechst 33342) was used to define the nuclear regions using the threshold tool and converted to a binary image. The erode and dilate binary functions were applied once to smooth the regions prior to applying the create selection function. The selection was added to the region of interest manager and then split into its separate constituents. Only regions that encompassed one full nucleus were retained. These regions were transferred to the SON channel where the fluorescence intensity was measured.

To assess total fluorescence within a cell, background was subtracted as described in the previous paragraph. The Cetn channel was thresholded to generate a binary image encompassing all the cell boundaries. This was subjected to the erode, dilate, and fill holes binary functions followed by applying the create selection function. The selection was added to the region of interest manager and then transferred to the channel to be quantified.

To measure the proximity of MTs to centrosomes in SIM reconstructions, line scan measurements of fluorescence intensity were employed beginning at the center of the centriole signal. The line was rotated 45°, generating eight measurements for each centriole. Each line scan measurement was then normalized to one at the initiating measurement at the centriole center prior to averaging all the line scans for each condition.

Statistical methods and data collection
Centriole counts, where a normal distribution is not predicted given the hard lower limit of centriole numbers, were compared using the Mann–Whitney test with two tails. Fluorescence intensity measurements were compared using an unpaired t test with a Welch correction. Statistics were calculated in Prism (Graphpad) except for radial analysis t tests, which were calculated in Excel (Microsoft) using the heteroscedastic comparison.

The investigators were not blinded when collecting data. Images were collected identically within experiments and data analysis was automated to the extent possible to prevent bias.

Flow cytometry
Cells were grown, treated with si RNAs, and S phase arrested as described above in 6-well plates (inoculum of 64,000 cells/well). To collect cells, media, PBS wash and trypsin-dissociated cells were combined into one tube per condition, spun, and washed with PBS and resuspended in Krishan stain (3.8 mM sodium citrate, 69 nM propidium iodide, 0.01% NP40, 0.01 mg/ml RNaseA)

(Krishan, 1975) and incubated at 4°C until run and analyzed by the University of Colorado Cancer Center Flow Cytometry Shared Resource on a Beckman Coulter FC500 flow cytometer. Cell cycle analysis was performed using ModFit LT software (Verity Software House, Topsham, ME).

RNA isolation, RT-PCR, and library preparation

RNA was isolated using the manufacturer's recommended protocols in three ways for the three replicates averaged in Figure 4C. Cytoplasmic RNA was isolated using the RNeasy Minikit (Qiagen) and the supplemental protocol provided by the manufacturer that includes a cell lysis step using buffer RLN and a step to separate nuclei from the cytoplasm by gentle centrifugation. RNA was also isolated using the Monarch Total RNA isolation miniprep kit (New England Biolabs). RNA was also extracted using the TRI Reagent (Thermo Fisher Scientific). cDNA was generated using 1 µg RNA, random hexamers (Thermo Fisher Scientific SO142), and Super-Script III Reverse Transcriptase (Thermo Fisher Scientific 18080044). Primers for PCR were ACTB-F: AGAGCTACGAGCTGCCTGAC; ACTB-R: AGCACTGTGTTGGCGTACAG; CNTROB-4F: TGCAA-GACTTGTCTCCATCTAGCTC; CNTROB-5R: TTGTCCAGTTGTTC-AATCATGGTATCTTTC; CNTROB-9F: AGAAGAGCCAGAGGG-AAGCC; CNTROB-10R: TTGCCGTAGGCTGCTCTCC; CEP131-4F: ACGGAGCCCACAGACTTCC; CEP131-6R: CGCAGTTGCCC-ACTGCTC; CEP131-14F: TGGGGTCCGAGGTGAGC; CEP131-15R: GCTGGATGGTGGCCTCG; KATNB1 2F: ATTTTGTGGG-TGGGGCTTCA; KATNB1 3R: TGATGGACCACAGGTTGACG; KATNB1 8F: TCGAGTTTCACCCCAACGAG; KATNB1 10R: CACATCAAAGCACCGCTCAG. Bands were quantified using Fiji (Schindelin et al., 2012).

RNA used for polyA-selected library generation for mRNA sequencing was isolated with the Monarch Total RNA isolation miniprep kit (New England Biolabs). Libraries were constructed using the Nugen Universal Plus mRNA-SEQ library construction kit (Nugen 0508) and sequenced on an Illumina NovaSEQ 6000 sequencer by the Genomics and Microarray shared resource at the University of Colorado Cancer Center.

Bioinformatics

RNA-seq libraries were sequenced on an Illumina NovaSeq 6000 (2 × 150) to a depth of 60–100 million paired-end reads. Reads were trimmed using cutadapt (v1.16) to remove adapters and aligned to the hg38 genome using STAR (v2.5.2a, Dobin et al., 2013). Gene counts were calculated using featureCounts (v1.6.2, Liao et al., 2014). Differentially expressed genes were identified for cells expressing SON siRNA and siControl cells (three replicates each) using DESeq2 (v1.28.1, Love et al., 2014). To compare annotated GO terms alongside our custom gene lists, we generated a custom Gene Matrix Transposed (.gmt) file containing CC GO terms (v7.1) along with the CD and centriolar satellites gene lists. To identify GO terms, genes down-regulated after SON knockdown (adjusted p value < 0.05, log2-fold change < -0.4) were sorted by p value and submitted as an ordered query using the R package gprofiler2 (v0.2.0, Kolberg et al., 2020).

Genes with changes in alternative splicing events were identified using rMATS (v4.1.0, Shen et al., 2014). Splicing events were identified using both junction and exon read counts and filtered to only include those with an FDR < 0.05 and where the absolute inclusion difference was > 0.4. GO terms were identified as described above.

Changes in alternative splicing were also analyzed using the software package, MAJIQ (v1.1.7a, Vaquero-Garcia et al., 2016). MAJIQ calculates the change in PSI (percentage spliced in) for splicing events between samples. The MAJIQ results were filtered to only include those where the change in PSI after SON knockdown was > 0.2. GO terms were identified as described above.

EM tomography

Cells were grown on sapphire disks and prepared for EM using high pressure freezing and freeze substitution (McDonald et al., 2010). Briefly, 3-mm sapphire disks (Technotrade International) were coated with gold. A large F was then scratched into the surface to help orient the cell side. The disks were coated with collagen and sterilized under UV light, and cells were plated for culturing as described above. Monolayers of cells grown on sapphire disks were then frozen using a Wohlwend Compact02 high-pressure freezer (Technotrade International). The frozen cells were then freeze-substituted in 1% OsO4 and 0.1% uranyl acetate in acetone at –80°C for 3 d, then gradually warmed to room temperature. The disks were then flat-embedded in a thin layer of Epon resin and polymerized at 60°C. Regions containing cells were identified in the light microscope, and a small square of resin containing the cells was excised and remounted onto a blank resin block. The cells were then sectioned en face and serial, thick sections (250–300 nm) were collected onto formvar-coated slot grids. Some grids were poststained with 2% uranyl acetate and Reynold's lead citrate; 15 nm colloidal gold (BBI International) was affixed to the section surface to serve as alignment markers.

Tomography was performed using a Tecnai F30 microscope operating at 300 kV (Thermo Fisher Scientific, Waltham, MA). Dual-axis tilt series were collected over a ±60° range using the SerialEM image acquisition software (Mastronarde, 2005) and a Gatan OneView camera (Gatan, Inc., Pleasanton, CA). For some datasets, tilt series were collected from two to four serial sections to reconstruct a larger volume of cell data. Tomograms were computed, serial tomograms were joined, and cellular features were modeled using the IMOD 4.9 software package (https://bio3d.colorado.edu/imod/; Kremer et al., 1996; Mastronarde, 1997).

MTs, centrioles, procentrioles, and positions of MT ends were manually traced in these reconstructions using the 3dmod program in the IMOD software package (Kremer et al., 1996). The slicer window in 3dmod was used to rotate a slice of image data containing the procentriole to view the MT organization in cross or longitudinal view. Models were projected in 3D to show the arrangement of the forming procentrioles in the centrosomes and the position of MTs and their ends within the volume. The places of close approach between MT ends to the centriole surface were identified with the MTK program in the IMOD suite. For this analysis, a single point at the minus end of each MT was modeled. The mother centriole was modeled as a series of closed contours to represent its surface. The MTK program uses models of MT ends to identify points of close apposition to the centriole and outputs a model object at each point of close approach. Measurements of the lengths of the close approach model contours were then extracted using the imodinfo program in the IMOD suite. The 3D distance between MT ends and a single reference point marking the center of the centriole was determined using the imod-dist program in the IMOD suite. The imod-dist program was then used to compute the 3D distances between the centriole and the locations of MT ends. In total, centrosomes from four siControl and four siSON cells were reconstructed and modeled in a total of 10 tomograms.

REFERENCES

Abramczuk MK, Burkard TR, Rolland V, Steinmann V, Duchek P, Jiang Y, Wissel S, Reichert H, Knoblich JA (2017). The splicing co-factor Barricade/Tat-SF1 is required for cell cycle and lineage progression in Drosophila neural stem cells. Development 144, 3932–3945.

Ahn E-Y, DeKelver RC, Lo M-C, Nguyen TA, Matsuura S, Boyapati A, Pandit S, Fu X-D, Zhang D-E (2011). SON controls cell-cycle progression by coordinated regulation of RNA splicing. Mol Cell 42, 185–198.

Azimzadeh J, Hergert P, Delouvée A, Euteneuer U, Formstecher E, Khodjakov A, Bornens M (2009). hPOC5 is a centrin-binding protein required for assembly of full-length centrioles. J Cell Biol 185, 101–114.

Balestra FR, Strnad P, Flückiger I, Gönczy P (2013). Discovering regulators of centriole biogenesis through siRNA-based functional genomics in human cells. Dev Cell 25, 555–571.

Canman JC, Hoffman DB, Salmon ED (2000). The role of pre- and post-anaphase microtubules in the cytokinesis phase of the cell cycle. Curr Biol 10, 611–614.

Chamling X, Seo S, Searby CC, Kim G, Slusarski DC, Sheffield VC (2014). The centriolar satellite protein AZI1 interacts with BBS4 and s the BBSome. PLoS Genet 10, e1004083.

Chen HY, Kelley RA, Li T, Swaroop A (2021). Primary cilia biogenesis and associated retinal ciliopathies. Semin Cell Dev Biol 110, 70–88.

Chia N-Y, Chan YS, Feng B, Lu X, Orlov YL, Moreau D, Kumar P, Yang L, Jiang J, Lau MS, et al. (2010). A genome-wide RNAi screen reveals determinants of human embryonic stem cell identity. Nature 468, 316–320.

Chiu Y, Ouyang P (2006). Loss of Pnn expression attenuates expression levels of SR family splicing factors and modulates alternative pre-mRNA splicing in vivo. Biochem Biophys Res Commun 341, 663–671.

Colicino EG, Hehnly H (2018). Regulating a key mitotic regulator, polo-like kinase 1 (PLK1). Cytoskelet Hoboken Nj 75, 481–494.

Conkar D, Bayraktar H, Firat-Karalar EN (2019). Centrosomal and ciliary targeting of CCDC66 requires cooperative action of centriolar satellites, microtubules and molecular motors. Sci Rep 9, 1–17.

Dahl KD, Sankaran DG, Bayless BA, Pinter ME, Galati DF, Heasley LR, Giddings TH, Pearson CG (2015). A short CEP135 splice isoform controls centriole duplication. Curr Biol CB 25, 2591–2596.

Dammermann A, Merdes A (2002). Assembly of centrosomal proteins and microtubule organization depends on PCM-1. J Cell Biol 159, 255–266.

Delaval B, Doxsey SJ (2010). Pericentrin in cellular function and disease. J Cell Biol 188, 181–190.

Denu RA, Sass MM, Johnson JM, Potts GK, Choudhary A, Coon JJ, Burkard ME (2019). Polo-like kinase 4 maintains centriolar satellite integrity by phosphorylation of centrosomal protein 131 (CEP131). J Biol Chem, jbc.RA118.004867.

Dictenberg JB, Zimmerman W, Sparks CA, Young A, Vidair C, Zheng Y, Carrington W, Fay FS, Doxsey SJ (1998). Pericentrin and γ-tubulin form a protein complex and are organized into a novel lattice at the centrosome. J Cell Biol 141, 163–174.

Dobin A, Davis CA, Schlesinger F, Drenkow J, Zaleski C, Jha S, Batut P, Chaisson M, Gingeras TR (2013). STAR: ultrafast universal RNA-seq aligner. Bioinforma Oxf Engl 29, 15–21.

Dominguez D, Tsai Y-H, Weatheritt R, Wang Y, Blencowe BJ, Wang Z (2016). An extensive program of periodic alternative splicing linked to cell cycle progression. ELife 5, e10288.

Galati DF, Sullivan KD, Pham AT, Espinosa JM, Pearson CG (2018). Trisomy 21 represses cilia formation and function. Dev Cell 46, 641–650.e6.

Ganapathi Sankaran D, Stemm-Wolf AJ, Pearson CG (2019). CEP135 isoform dysregulation promotes centrosome amplification in breast cancer cells. Mol Biol Cell 30, 1230–1244.

Ganem NJ, Godinho SA, Pellman D (2009). A mechanism linking extra centrosomes to chromosomal instability. Nature 460, 278–282.

Gheiratmand L, Coyaud E, Gupta GD, Laurent EM, Hasegan M, Prosser SL, Gonçalves J, Raught B, Pelletier L (2019). Spatial and proteomic profiling reveals centrosome-independent features of centriolar satellites. EMBO J, e101109.

Gillingham AK, Munro S (2000). The PACT domain, a conserved centrosomal targeting motif in the coiled-coil proteins AKAP450 and pericentrin. EMBO Rep 1, 524–529.

Godinho SA, Picone R, Burute M, Dagher R, Su Y, Leung CT, Polyak K, Brugge JS, Théry M, Pellman D (2014). Oncogene-like induction of cellular invasion from centrosome amplification. Nature 510, 167–171.

Gönczy P, Hatzopoulos GN (2019). Centriole assembly at a glance. J Cell Sci 132, jcs228833.

Gossen M, Freundlieb S, Bender G, Müller G, Hillen W, Bujard H (1995). Transcriptional activation by tetracyclines in mammalian cells. Science 268, 1766–1769.

Graser S, Stierhof Y-D, Lavoie SB, Gassner OS, Lamla S, Le Clech M, Nigg EA (2007). Cep164, a novel centriole appendage protein required for primary cilium formation. J Cell Biol 179, 321–330.

Gudi R, Haycraft CJ, Bell PD, Li Z, Vasu C (2015). centrobin-mediated regulation of the centrosomal protein 4.1-associated protein (CPAP) level limits centriole length during elongation stage. J Biol Chem 290, 6890–6902.

Gudi R, Zou C, Dhar J, Gao Q, Vasu C (2014). centrobin-centrosomal protein 4.1-associated Protein (CPAP) Interaction Promotes CPAP localization to the centrioles during centriole duplication. J Biol Chem 289, 15166–15178.

Gudi R, Zou C, Li J, Gao Q (2011). centrobin–tubulin interaction is required for centriole elongation and stability. J Cell Biol 193, 711–725.

Gupta GD, Coyaud É, Gonçalves J, Mojarad BA, Liu Y, Wu Q, Gheiratmand L, Comartin D, Tkach JM, Cheung SW, et al. (2015). A dynamic protein interaction landscape of the human centrosome-cilium interface. Cell 163, 1484–1499.

Hatch EM, Kulukian A, Holland AJ, Cleveland DW, Stearns T (2010). Cep152 interacts with Plk4 and is required for centriole duplication. J Cell Biol 191, 721–729.

Hickey CJ, Kim J-H, Ahn E-YE (2014). New discoveries of old SON: A link between RNA splicing and cancer. J Cell Biochem 115, 224–231.

Hori A, Barnouin K, Snijders AP, Toda T (2016). A non-canonical function of Plk4 in centriolar satellite integrity and ciliogenesis through PCM1 phosphorylation. EMBO Rep 17, 326–337.

Hori A, Peddie CJ, Collinson LM, Toda T (2015). Centriolar satellite– and hMsd1/SSX2IP-dependent microtubule anchoring is critical for centriole assembly. Mol Biol Cell 26, 2005–2019.

Hu WF, Pomp O, Ben-Omran T, Kodani A, Henke K, Mochida GH, Yu TW, Woodworth MB, Bonnard C, Raj GS, et al. (2014). Katanin p80 regulates human cortical development by limiting centriole and cilia number. Neuron 84, 1240–1257.

Huen MSY, Sy SMH, Leung KM, Ching Y-P, Tipoe GL, Man C, Dong S, Chen J (2010). SON is a spliceosome-associated factor required for mitotic progression. Cell Cycle 9, 2679–2685.

Ilik A, Malszycki M, Lübke AK, Schade C, Meierhofer D, Akta T (2020). SON and SRRM2 are essential for nuclear speckle formation. ELife 9, e60579.

Ito D, Zitouni S, Jana SC, Duarte P, Surkont J, Carvalho-Santos Z, Pereira-Leal JB, Ferreira MG, Bettencourt-Dias M (2019). Pericentrin-mediated SAS-6 recruitment promotes centriole assembly. ELife 8, e41418.

Jeffery JM, Grigoriev I, Poser I, van der Horst A, Hamilton N, Waterhouse N, Bleier J, Subramaniam VN, Maly IV, Akhmanova A, Khanna KK (2013). centrobin regulates centrosome function in interphase cells by limiting pericentriolar matrix recruitment. Cell Cycle 12, 899–906.

Jiao AL, Perales R, Umbreit NT, Haswell JR, Piper ME, Adams BD, Pellman D, Kennedy S, Slack FJ (2019). Human nuclear RNAi-defective 2 (NRDE2) is an essential RNA splicing factor. RNA 25, 352–363.

Kim DH, Ahn JS, Han HJ, Kim HM, Hwang J, Lee KH, Cha-Molstad H, Ryoo IJ, Jang JH, Ko SK, et al. (2019). Cep131 overexpression promotes centrosome amplification and colon cancer progression by regulating Plk4 stability. Cell Death Dis 10, 570.

Kim J-H, Shinde DN, Reijnders MRF, Hauser NS, Belmonte RL, Wilson GR, Bosch DGM, Bubulya PA, Shashi V, Petrovski S, et al. (2016). De Novo Mutations in SON Disrupt RNA splicing of genes essential for brain development and metabolism, causing an intellectual-disability syndrome. Am J Hum Genet 99, 711–719.

Kim T-S, Park JE, Shukla A, Choi S, Murugan RN, Lee JH, Ahn M, Rhee K, Bang JK, Kim BY, et al. (2013). Hierarchical recruitment of Plk4 and regulation of centriole biogenesis by two centrosomal scaffolds, Cep192 and Cep152. Proc Natl Acad Sci USA 110, E4849–E4857.

Kitagawa D, Vakonakis I, Olieric N, Hilbert M, Keller D, Olieric V, Bortfeld M, Erat MC, Flückiger I, Gönczy P, Steinmetz MO (2011). Structural basis of the 9-fold symmetry of centrioles. Cell 144, 364–375.

Kleylein-Sohn J, Westendorf J, Clech ML, Habedanck R, Stierhof Y-D, Nigg EA (2007). Plk4-induced centriole biogenesis in human cells. Dev Cell 13, 190–202.

Kodani A, Yu TW, Johnson JR, Jayaraman D, Johnson TL, Al-Gazali L, Sztriha L, Partlow JN, Kim H, Krup AL, et al. (2015). Centriolar satellites assemble centrosomal microcephaly proteins to recruit CDK2 and promote centriole duplication. ELife, e07519.

Kolberg L, Raudvere U, Kuzmin I, Vilo J, Peterson H (2020). gprofiler2—an R package for gene list functional enrichment analysis and namespace conversion toolset g:Profiler. F1000Research 9, 709.

Kremer JR, Mastronarde DN, McIntosh JR (1996). Computer visualization of three-dimensional image data using IMOD. J Struct Biol 116, 71–76.

Krishan A (1975). Rapid flow cytofluorometric analysis of mammalian cell cycle by propidium iodide staining. J Cell Biol 66, 188–193.

Kubo A, Sasaki H, Yuba-Kubo A, Tsukita S, Shiina N (1999). Centriolar satellites. J Cell Biol 147, 969–980.

Kurokawa K, Akaike Y, Masuda K, Kuwano Y, Nishida K, Yamagishi N, Kajita K, Tanahashi T, Rokutan K (2014). Downregulation of serine/arginine-rich splicing factor 3 induces G1 cell cycle arrest and apoptosis in colon cancer cells. Oncogene 33, 1407–1417.

Kurtulmus B, Wang W, Ruppert T, Neuner A, Cerikan B, Viol L, Sanchez RD, Gruss OJ, Pereira G (2015). WDR8 is a centriolar satellite and centriole-associate protein that promotes ciliary vesicle docking during ciliogenesis. J Cell Sci, jcs.179713.

Leda M, Holland AJ, Goryachev AB (2018). Autoamplification and competition drive symmetry breaking: initiation of centriole duplication by the PLK4-STIL network. IScience 8, 222–235.

Lee S-H, Joo K, Jung EJ, Hong H, Seo J, Kim J (2017). Export of membrane proteins from the Golgi complex to the primary cilium requires the kinesin motor, KIFC1. FASEB J fj.201700563R.

Leidel S, Delattre M, Cerutti L, Baumer K, Gönczy P (2005). SAS-6 defines a protein family required for centrosome duplication in C. elegans and in human cells. Nat Cell Biol 7, 115–125.

Levine MS, Bakker B, Boeckx B, Moyett J, Lu J, Vitre B, Spierings DC, Lansdorp PM, Cleveland DW, Lambrechts D, et al. (2017). Centrosome amplification is sufficient to promote spontaneous tumorigenesis in mammals. Dev Cell 40, 313–322.e5.

Liao Y, Smyth GK, Shi W (2014). featureCounts: an efficient general purpose program for assigning sequence reads to genomic features. Bioinforma Oxf Engl 30, 923–930.

Lin Y-C, Chang C-W, Hsu W-B, Tang C-JC, Lin Y-N, Chou E-J, Wu C-T, Tang TK (2013a). Human microcephaly protein CEP135 binds to hSAS-6 and CPAP, and is required for centriole assembly. EMBO J 32, 1141–1154.

Lin Y-N, Wu C-T, Lin Y-C, Hsu W-B, Tang C-JC, Chang C-W, Tang TK (2013b). CEP120 interacts with CPAP and positively regulates centriole elongation. J Cell Biol 202, 211–219.

Liu Y, Gupta GD, Barnabas DD, Agircan FG, Mehmood S, Wu D, Coyaud E, Johnson CM, McLaughlin SH, Andreeva A, et al. (2018). Direct binding of CEP85 to STIL ensures robust PLK4 activation and efficient centriole assembly. Nat Commun 9, 1731.

Loncarek J, Bettencourt-Dias M (2018). Building the right centriole for each cell type. J Cell Biol 217, 823–835.

Love MI, Huber W, Anders S (2014). Moderated estimation of fold change and dispersion for RNA-seq data with DESeq2. Genome Biol 15, 550.

Lu X, Göke J, Sachs F, Jacques P-É, Liang H, Feng B, Bourque G, Bubulya PA, Ng H-H (2013). SON connects the splicing-regulatory network with pluripotency in human embryonic stem cells. Nat Cell Biol 15, 1141–1152.

Marteil G, Guerrero A, Vieira AF, de Almeida BP, Machado P, Mendonça S, Mesquita M, Villarreal B, Fonseca I, Francia ME, et al. (2018). Over-elongation of centrioles in cancer promotes centriole amplification and chromosome missegregation. Nat Commun 9, 1258.

Mastronarde DN (1997). Dual-axis tomography: an approach with alignment methods that preserve resolution. J Struct Biol 120, 343–352.

Mastronarde DN (2005). Automated electron microscope tomography using robust prediction of specimen movements. J Struct Biol 152, 36–51.

Matsuo K, Ohsumi K, Iwabuchi M, Kawamata T, Ono Y, Takahashi M (2012). Kendrin is a novel substrate for separase involved in the licensing of centriole duplication. Curr Biol 22, 915–921.

McDonald K, Schwarz H, Müller-Reichert T, Webb R, Buser C, Morphew M (2010). "Tips and tricks" for high-pressure freezing of model systems. Methods Cell Biol 96, 671–693.

McLamarrah TA, Buster DW, Galletta BJ, Boese CJ, Ryniawec JM, Hollingsworth NA, Byrnes AE, Brownlee CW, Slep KC, Rusan NM, Rogers GC (2018). An ordered pattern of Ana2 phosphorylation by Plk4 is required for centriole assembly. J Cell Biol jcb.201605106.

McNally KP, Bazirgan OA, McNally FJ (2000). Two domains of p80 katanin regulate microtubule severing and spindle pole targeting by p60 katanin. J Cell Sci 113, 1623–1633.

Mitchison HM, Valente EM (2017). Motile and non-motile cilia in human pathology: from function to phenotypes. J Pathol 241, 294–309.

Moldrich RX, Dauphinot L, Laffaire J, Rossier J, Potier M-C (2007). Down syndrome gene dosage imbalance on cerebellum development. Prog Neurobiol 82, 87–94.

Moyer TC, Clutario KM, Lambrus BG, Daggubati V, Holland AJ (2015). Binding of STIL to Plk4 activates kinase activity to promote centriole assembly. J Cell Biol 209, 863–878.

Moyer TC, Holland AJ (2019). PLK4 promotes centriole duplication by phosphorylating STIL to link the procentriole cartwheel to the microtubule wall. ELife 8, e46054.

Nigg EA, Holland AJ (2018). Once and only once: mechanisms of centriole duplication and their deregulation in disease. Nat Rev Mol Cell Biol 19, 297–312.

Odabasi E, Gul S, Kavakli IH, Firat-Karalar EN (2019). Centriolar satellites are required for efficient ciliogenesis and ciliary content regulation. EMBO Rep, e47723.

Ohta M, Ashikawa T, Nozaki Y, Kozuka-Hata H, Goto H, Inagaki M, Oyama M, Kitagawa D (2014). Direct interaction of Plk4 with STIL ensures formation of a single procentriole per parental centriole. Nat Commun 5, 5267.

Ohta M, Watanabe K, Ashikawa T, Nozaki Y, Yoshiba S, Kimura A, Kitagawa D (2018). Bimodal Binding of STIL to Plk4 controls proper centriole copy number. Cell Rep 23, 3160–3169.e4.

Park EM, Scott PM, Clutario K, Cassidy KB, Zhan K, Gerber SA, Holland AJ (2020). WBP11 is required for splicing the TUBGCP6 pre-mRNA to promote centriole duplication. J Cell Biol 219, e201904203.

Park J-E, Zhang L, Bang JK, Andresson T, DiMaio F, Lee KS (2019). Phase separation of Polo-like kinase 4 by autoactivation and clustering drives centriole biogenesis. Nat Commun 10, 4959.

Penev A, Bazley A, Shen M, Boeke JD, Savage SA, Sfeir A (2021). Alternative splicing is a developmental switch for hTERT expression. Mol Cell 81, 2349–2360.e6.

Prosser SL, Pelletier L (2020). Centriolar satellite biogenesis and function in vertebrate cells. J Cell Sci 133, jcs239566.

Puklowski A, Homsi Y, Keller D, May M, Chauhan S, Kossatz U, Grünwald V, Kubicka S, Pich A, Manns MP, et al. (2011). The SCF–FBXW5 E3-ubiquitin ligase is regulated by PLK4 and targets HsSAS-6 to control centrosome duplication. Nat Cell Biol 13, 1004–1009.

Reina J, Gottardo M, Riparbelli MG, Llamazares S, Callaini G, Gonzalez C (2018). centrobin is essential for C-tubule assembly and flagellum development in Drosophila melanogaster spermatogenesis. J Cell Biol 217, 2365–2372.

Reiter JF, Leroux MR (2017). Genes and molecular pathways underpinning ciliopathies. Nat Rev Mol Cell Biol 18, 533–547.

Roper RJ, Baxter LL, Saran NG, Klinedinst DK, Beachy PA, Reeves RH (2006). Defective cerebellar response to mitogenic Hedgehog signaling in Down's syndrome mice. Proc Natl Acad Sci USA 103, 1452–1456.

Sanchez AD, Feldman JL (2017). Microtubule-organizing centers: from the centrosome to non-centrosomal sites. Curr Opin Cell Biol 44, 93–101.

Sankaran DG, Stemm-Wolf AJ, McCurdy BL, Hariharan B, Pearson CG (2020). A semi-automated machine learning-aided approach to quantitative analysis of centrosomes and microtubule organization. J Cell Sci 133, jcs243543.

Schindelin J, Arganda-Carreras I, Frise E, Kaynig V, Longair M, Pietzsch T, Preibisch S, Rueden C, Saalfeld S, Benjamin S, et al. (2012). Fiji: an open-source platform for biological-image analysis. Nat Methods 9, 676–682.

Schmidt TI, Kleylein-Sohn J, Westendorf J, Le Clech M, Lavoie SB, Stierhof Y-D, Nigg EA (2009). Control of centriole length by CPAP and CP110. Curr Biol 19, 1005–1011.

Schöckel L, Möckel M, Mayer B, Boos D, Stemmann O (2011). Cleavage of cohesin rings coordinates the separation of centrioles and chromatids. Nat Cell Biol 13, 966–972.

Sharma A, Markey M, Torres-Muñoz K, Varia S, Kadakia M, Bubulya A, Bubulya PA (2011). Son maintains accurate splicing for a subset of human pre-mRNAs. J Cell Sci 124, 4286–4298.

Shen S, Park JW, Lu Z, Lin L, Henry MD, Wu YN, Zhou Q, Xing Y (2014). rMATS: Robust and flexible detection of differential alternative splicing from replicate RNA-Seq data. Proc Natl Acad Sci USA 111, E5593–E5601.

Siebring-van Olst E, Blijlevens M, de Menezes RX, van der Meulen-Muileman IH, Smit EF, van Beusechem VW (2017). A genome-wide siRNA screen

for regulators of tumor suppressor p53 activity in human non-small cell lung cancer cells identifies components of the RNA splicing machinery as targets for anticancer treatment. Mol Oncol 11, 534–551.

Silkworth WT, Nardi IK, Scholl LM, Cimini D (2009). Multipolar spindle pole coalescence is a major source of kinetochore mis-attachment and chromosome mis-segregation in cancer cells. PLoS One 4, e6564.

Sonnen KF, Gabryjonczyk A-M, Anselm E, Stierhof Y-D, Nigg EA (2013). Human Cep192 and Cep152 cooperate in Plk4 recruitment and centriole duplication. J Cell Sci 126, 3223–3233.

Spektor A, Tsang WY, Khoo D, Dynlacht BD (2007). Cep97 and CP110 suppress a cilia assembly program. Cell 130, 678–690.

Staples CJ, Myers KN, Beveridge RDD, Patil AA, Lee AJX, Swanton C, Howell M, Boulton SJ, Collis SJ (2012). The centriolar satellite protein Cep131 is important for genome stability. J Cell Sci 125, 4770–4779.

Stearns T, Evans L, Kirschner M (1991). γ-Tubulin is a highly conserved component of the centrosome. Cell 65, 825–836.

Suvorova ES, Croken M, Kratzer S, Ting L-M, Felipe MCde, Balu B, Markillie ML, Weiss LM, Kim K, White MW (2013). Discovery of a splicing regulator required for cell cycle progression. PLoS Genet 9, e1003305.

Tanackovic G, Krämer A (2005). Human splicing factor SF3a, but not SF1, is essential for pre-mRNA splicing in vivo. Mol Biol Cell 16, 1366–1377.

Thawani A, Stone HA, Shaevitz JW, Petry S (2019). Spatiotemporal organization of branched microtubule networks. ELife 8, e43890.

Tokita MJ, Braxton AA, Shao Y, Lewis AM, Vincent M, Küry S, Besnard T, Isidor B, Latypova X, Bézieau S, et al. (2016). De Novo truncating variants in SON cause intellectual disability, congenital malformations, and failure to thrive. Am J Hum Genet 99, 720–727.

Tovey CA, Conduit PT (2018). Microtubule nucleation by γ-tubulin complexes and beyond. Essays Biochem, EBC20180028.

Tsou M-FB, Wang W-J, George KA, Uryu K, Stearns T, Jallepalli PV (2009). Polo kinase and separase regulate the mitotic licensing of centriole duplication in human cells. Dev Cell 17, 344–354.

Urlaub H, Raker VA, Kostka S, Lührmann R (2001). Sm protein–Sm site RNA interactions within the inner ring of the spliceosomal snRNP core structure. EMBO J 20, 187–196.

Vaquero-Garcia J, Barrera A, Gazzara MR, González-Vallinas J, Lahens NF, Hogenesch JB, Lynch KW, Barash Y (2016). A new view of transcriptome complexity and regulation through the lens of local splicing variations. ELife 5, e11752.

Vulprecht J, David A, Tibelius A, Castiel A, Konotop G, Liu F, Bestvater F, Raab MS, Zentgraf H, Izraeli S, Krämer A (2012). STIL is required for centriole duplication in human cells. J Cell Sci 125, 1353–1362.

Wickramasinghe VO, Gonzàlez-Porta M, Perera D, Bartolozzi AR, Sibley CR, Hallegger M, Ule J, Marioni JC, Venkitaraman AR (2015). Regulation of constitutive and alternative mRNA splicing across the human transcriptome by PRPF8 is determined by 5′ splice site strength. Genome Biol 16, 201.

Wu C-T, Chen H-Y, Tang TK (2018). Myosin-Va is required for preciliary vesicle transportation to the mother centriole during ciliogenesis. Nat Cell Biol 20, 175–185.

Xu X, Huang S, Zhang B, Huang F, Chi W, Fu J, Wang G, Li S, Jiang Q, Zhang C (2017). DNA replication licensing factor Cdc6 and Plk4 kinase antagonistically regulate centrosome duplication via Sas-6. Nat Commun 8, 15164.

Yamamoto S, Kitagawa D (2019). Self-organization of Plk4 regulates symmetry breaking in centriole duplication. Nat Commun 10, 1810.

Yang TT, Chong WM, Wang WJ, Mazo G, Tanos B, Chen Z, Tran TMN, Chen YD, Weng RR, Huang CE, et al. (2018). Super-resolution architecture of mammalian centriole distal appendages reveals distinct blade and matrix functional components. Nat Commun 9, 2023.

Youn YH, Han Y-G (2018). Primary cilia in brain development and diseases. Am J Pathol 188, 11–22.

Young A, Dictenberg JB, Purohit A, Tuft R, Doxsey SJ (2000). Cytoplasmic dynein-mediated assembly of pericentrin and γ tubulin onto centrosomes. Mol Biol Cell 11, 2047.

Zhang C-Z, Spektor A, Cornils H, Francis JM, Jackson EK, Liu S, Meyerson M, Pellman D (2015). Chromothripsis from DNA damage in micronuclei. Nature 522, 179–184.

Zou C, Li J, Bai Y, Gunning WT, Wazer DE, Band V, Gao Q (2005). centrobin. J Cell Biol 171, 437–445.